Crystal growth, structure and physical properties of crystals

Kurazhkovskaya V.S., Dorokhova G.I., Zykova T.B. Change of vezuvianit structural peculiarity at isomorphism.

M.V. Lomonosov Moscow State University, Geological Department, Vorobjovy Gory, Moscow, 119899, Russia crystal@geol.msu.ru

key words: [*vezuvianite, infrared spectroscopy, isomorphism*]

Vesuvianite is an ortho-diorthosilicate of a general schematic formula $X_{\sim19}Y_{13}Z_{18}O_{68}W_{10}$, where X – Ca and other cations, which occupy sites of coordination number 8, Y – cations occupying octahedrons and pentagonal polyhedrons: Al, Fe, Mg, Ti, etc., Z – Si in tetrahedrons, Table 1.

W – univalent and bivalent anions. Structures of vesuvianites are studied in dependence on a character of cation ordering in different sites within three space groups: $P4/nnc$ and its two sub-groups $P4nc$ (C_{4v}) and $P4/n$ (C_{4h}). It is found earlier [1, 2], that two "garnet blocks" (GB), i.e. volume bar, outsets from the grossular garnet structure, are the basis of the vesuvianite structure. Junction of two GB leads to formation of diorthogroups $[Si_2O_7]$. Cation composition of GB $\{Ca_{18}Al_8Si_{18}\}$ is practically constant. Cations of the "vesuvianite filling" (VF) occupy cavities formed within the frame-work. Isomorphic substitutions are characteristic feature of VF (Table 1). Hypothetical position R is suggested for vesuvianites with an excess cations (>19).

CN	Garnet block (GB)				Vezuvianite filling (VF)			
		Positions of cations						
8	$(Ca1)_2$	$(Ca2)_8$	$(Ca3)_8$		$(Ca4)_1$			
6			$(Al1)_8$			$(Al2)_4$		$(R?)_{2 \, and >}$
5							$(Al3)_1$	

Table 2.

N of sample	$(Ca4)_1$	$(Al2)_4$	$(Al3)_1$	$(R?)_{2 \, and >}$
		Positions of "vezuvianite filling"		
1	Ca_1	$Al_{2.93}Fe_{1.07}$	$Ca_{0.66}Na_{0.34}$	$Fe_{2.1}Mn_{0.11}$
2	Ca_1	$Al_{3.72}Fe_{0.24}Ti_{0.04}$	$Ca_{0.58}Na_{0.23}Mg_{0.14}Zn_{0.05}$	$Fe_{0.38}Mg_{2.03}$
3	Ca_1	$Al_{2.16}Fe_{0.93}Ti_{0.92}$	$Ca_{0.92}Na_{0.39?}$	$Fe_{0.91}Mg_{1.88}Mn_{0.1}$
4	Ca_1	$Al_{1.16}Fe_{2.05}Mg_{0.84}$	$Ca_{0.61}Na_{0.18}Mn_{0.1}Zn_{0.02}$	$Mg_{2.12}$

Table 3.

| N of sample	ν_{as} Si-O-Si	ν_3 Si-O	ν_1 Si-O	ν_s Si-O-Si	ν_4 Si-O	ν Me^{VI}-O	ν_2 Si-O	$\Delta\nu_3$
				Infrared bands (cm^{-1})				
1	1020	980,990		800	635,575	475	440	80
2	1020	970,920	890	800	605,575	485	435	50
3	1020	975,915	860	800	595,570	470	430	60
4	1020	980,920		800	595,570	470	435	60

The present study shows the results of investigation of structural features of vesuvianites of different compositions with the excess of cations by the method of infrared spectroscopy. According to cation composition of VF (Table 2) and the character of infrared spectra (Fig. 1, Table 3), two groups of vesuvianites could be distinguished: (1) alumo-ferrous, magnesium-free or of low Mg and Ni content, and (2) magnesium-rich. Aluminum content prevails over Fe in the first group. The second group can be divided into the following sub-groups: alumo-magnesium of low Fe content, alumo-ferrous-magnesium, and ferrous-magnesium of low Al content. Variations of unit cell parameters are insignificant and a_0=15.554-5.578, c_0=11.796-11.805.

Splitting of bands of the valent ν_3 oscillations is 80 cm^{-1}, frequency values are higher than in the subsequent spectra. The latter fact implies that Fe in such samples is present as a trivalent form: size of Fe^{3+} is less then sizes of Mg and Fe^{2+}, whereas displacement of Si-O bands toward

low frequencies occurs by introduction of lager cations in to polyhedrons connected by apexes and edges. Alumomagnesium vesuvianite (2) shows a triplet of equally intensive bands in the basic spectrum. One band, 1020 cm^{-1}, is related to oscillation ν_{as} of the Si-O-Si bond in the diorthogroup. Splitting of ν_3 oscillations drops down to 50 cm^{-1}. Deformational ν_4 oscillations are displaced to low frequencies at 30 cm^{-1}. An abrupt decrease of splitting of the bands of ν_3 oscillations in magnesium-rich samples is similar to the process, which occurs in garnets at incorporation of larger cations into octahedron. A decrease of distortion of tetrahedrons with the positional symmetry S_4 takes place in this process. Apparently, the decrease of band splitting in vesuvianite is also related to the substitution $Fe^{3+} \rightarrow Mg$. An increase of Ti and Fe content in the Al2-position (3) causes a decrease of intensity of ν_3 oscillations, whereas band splitting increases up to 60cm^{-1}. Slight displacement (by 10 cm^{-1}) of the deformational

bands towards low frequencies occurs because of increase of cation sizes in the Al2 octahedrons. These octahedra are connected by apex with the tetrahedra of the diorthogroup. Difference in oscillations of one-phase and anti-phase tetrahedra of the diorthogroup increases at an increase of cation sizes. It causes the band splitting. A spectrum of a last ferrous-magnesium sample in the region of valent oscillations is presented by an intensive band of ν_{as} Si-O-Si oscillations, which is a background for 980cm^{-1} and 910 cm^{-1} bands. This spectrum is similar to the infrared spectrum of wiluite, boron-bearing vesuvianite, which contains bivalent Mg and Fe. Apparently, ferrous-magnesium samples also contain Mg and Fe^{2+} predominantly.

Thus, infrared study of vesuvianites showed delicate structural variations, related to distortions of SiO$_4$-tetrahedrons, caused by isomorphic substitutions in the cation positions of VF. Several types of infrared spectra of vesuvianites in dependence on composition were observed. Variations of spectral pattern in transition from vesuvianites, containing trivalent cations (Al, Fe^{3+}), to vesuvianites, dominated by bivalent cations (Mg, Fe^{2+}) were found. Table 3 shows a probable filling of the positions in the studied vesuvianites.
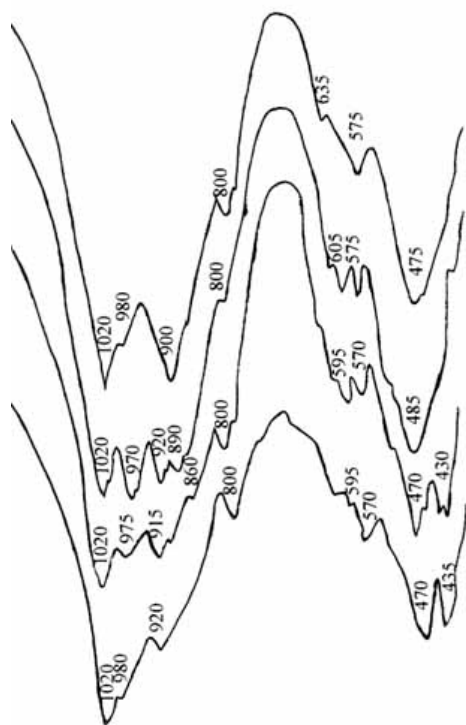
Reference:

1. G.I. Dorokhova, O.V. Kononov, T.B. Zykova, M.V. Silaev. Genetic and structural relationship of garnet and vezuvianite. Abstracts of International Conference "Spectroscopy, X-Ray diffraction and crystal chemistry of minerals", Kazan, 1997.
2. O.V. Kononov, G.I. Dorokhova, M.V. Silaev. The principles of systematic of vezuvianites. Abstracts of International Symposium of history of mineralogy and mineralogical museums, gemology, crystal chemistry and classification of minerals, St-Peterburg, 1998.

Kurazhkovskaya V.S., Dorohova G.I., Rosenberg К.A., Kabalov J.K. X-ray diffraction and infrared spectroscopy of Al-Cr-spinels.

M.V. Lomonosov Moscow State University, geological department, Vorobjovy Gory, Moscow, 119899, Russia crystal@geol.msu.ru

Spinel is a widespread high temperature natural mineral with general composition A^{2+}B$_2^{3+}$O$_4$. The normal spinel's space group is $Fd3m(O_h)$, Z=8, with A^{2+} in tetrahedral and B^{3+} in octahedral coordination. Structural features of Cr-containing spinels (from the Urals) have been studied in this work using the methods of X-ray analysis and Infrared spectroscopy. MgAl-spinel (from the Pamirs) and hercinite (from the Hibins) were studied as well for the better understanding and interpretation of the changes in infrared spectra due to isomorphic cation substitutions in both tetrahedral and octahedral positions.

The microprobe analysis of spinels had been done with the electron microprobe Camebax SX-50 (Al-spinels) and JXA-5 (Cr-spinels). Powder X-ray diffraction was carried out with ADP diffractometer using Mo k$_\alpha$ radiation with Zr filter. Data were collected in step scan mode using a step of 0.025^o with counting time of 2s. Infrared spectra were recorded on the Specord-75IR spectrometer with KBr as window material in the frequency range from 1000-400 cm^{-1}.

The results are represented in table1 and in fig.1.

Vibrations in condensed metall-oxygen compounds can be divided into two groups,which are 1) vibrations of the light oxygen ions relative to the heavier A^{2+} and B^{3+} cations; and 2) vibrations of A^{2+} and B^{3+} cations relative to each other. In spinel (space group $Fd3m$ (O_h)) four three times degenerated F_{1u} vibrations are observed. In spinel structure each oxygen is shared between one tetrahedral and three octahedral cations. The symmetry of the oxygen position is $C3v$. Oxygen ions displace along 3-fold axis and perpendicular to it. When oxygen ions displace along the 3-fold axis vibrations F_{1u} (A^{2+}-O-3B^{3+}) occur. Vibrations of this type account for the intense high frequency infrared band. Displacements of oxygen ions normal to 3-fold axis involve B^{3+}-O-2B^{3+} stretching and produces F_{1u}^2 vibrations, which involve only octahedral cations. These vibrations account for the intense low frequency infrared band. The displacements of the cations relative to each other produce the low frequency vibrations that cannot be registered by the spectrometer used in this study.

The frequency of vibrations is determined by force constant, which is inversely related to the size and masses of ions. As seen in the table and at the fig. when Fe^{2+} ions substitute Mg in tetrahedral positions and Al is substituted by Cr and Fe^{3+}ions in octahedral positions we can see a regular increase in the size of unit cell and shifts of infrared bands to lower frequencies (table1, fig1). For instance, vibrations F_{1u}^1 (A^{2+}-O-3B^{3+}) in MgAl-spinel (sample 1) account for frequency 675cm^{-1}, and the same vibrations in Cr-spinel (sample 6) correspond to the frequency 610cm^{-1}. The higher frequency (650 cm^{-1}) of the F_{1u}^1 vibration in

hercinite (sample 2) is caused by the absence of big and heavy B^{3+} cations in octahedral coordination.

Spinels containing light cations such as Al show some anomalies in low frequency region of infrared spectrum. The Al ion participates more in the F_{1u}^2 (B^{3+}-O-$2B^{3+}$) vibration than does a heavier B^{3+} cation. As a result F_{1u}^2 and F_{1u}^3 vibrations approach each other more closely in frequency [1]. In the infrared spectrum of hercinite (fig.1,spectrum2) the band of F_{1u}^3 (Al-Al) vibrations shifts to the region of F_{1u}^2 vibrations. This spectrum reveals three intense bands: F_{1u}^1 – 650cm^{-1}, F_{1u}^2 – 555cm^{-1}, F_{1u}^3– 500cm^{-1}. Mg ions participate more in F_{1u}^3 vibration than do other heavier divalent cations, this causes F_{1u}^3 (Al-Al) vibration band and F_{1u}^4 (Mg-Mg) vibration band coming closer to each other. In the consequence the F_{1u}^3 band does not appear, its frequency is lower than 400 cm^{-1}. Due to participation of Al ions in the F_{1u}^2 vibration in the spectrum of MgAl-spinel the band F_{1u}^2 gets wider, more intense and shifts to the region of lower frequencies (555→515cm^{-1}); a low intense 575cm^{-1} band also appears (fig.1,spectrum1).

Fig.1. Infrared spectra of spinels.

When Al ions are partly substituted by Cr ions the F_{1u}^2 band shifts to lower frequencies (515→500cm^{-1}) due to the bigger size and heavier mass of Cr ions, compared to Al ions. Still high content of Al ions determines width and quite low frequencies of the F_{1u}^2 band and the appearance of the subsidiary shoulder at 548 cm^{-1} (fig.1, spectrum3). In the sample 4 Cr and Fe^{3+}ions occupy three forths of octahedral positions, and the contribution of Al ions to F_{1u}^2 vibrations is insignificant. The F_{1u}^2 band is narrow, its frequency remains and the subsidiary shoulder is absent. It can be assumed that this band accounts for B^{3+}-O-$2B^{3+}$ vibration without any contribution of Al-Al vibration. Futher occupation of octahedral positions by Fe^{3+} and Cr ions, as we have in the sample 5, causes insignificant shift (5cm^{-1}) of the F_{1u}^2 band to lower frequency region of the spectrum. In the spectrum of sample 6 this band has a 15cm^{-1} shift in spite of both Fe^{3+} and Cr ions content getting down. It is correlated with the three times increase of Fe^{3+}ions content, which are bigger and heavier than Cr ions.

Thus, X-ray and infrared spectroscopy study of Al and Cr spinels showed a relation between unit cell parameters, band's shifts in infrared spectra and isomorhous substitutions in tetrahedral and octahedral positions. The influence on infrared spectrum of chemical nature of atoms not only their size is shown. Anomalous vibrations of Al atoms In Mg-Al spinels and in Al-Cr spinels were revealed.
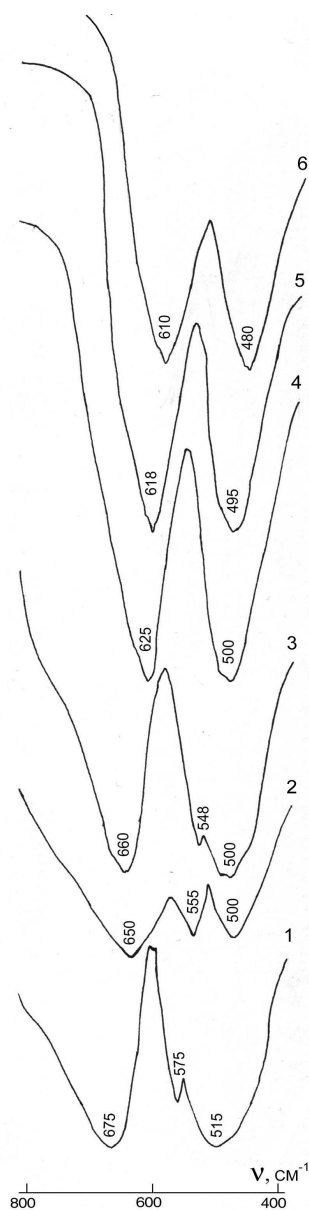
Table 1. Unit cell parameters and infrared bands of spinels

sample	Formula	Unit cell parameter, Å	Infrared bands, (cm^{-1})
1	$(Mg_{0.99}Fe_{0.01})(Al_{1.97}Fe_{0.03})O_4$	8.0261	675, 575, 515
2	$(Fe_{0.95}Mn_{0.03}Mg_{0.02})(Al_{1.97}Fe_{0.03})O_4$	8.1331	650, 555, 500
3	$(Fe_{0.295}Mg_{0.668}Ni_{0.006}Mn_{0.001}Ti_{0.001})(Al_{1.635}Cr_{0.394})O_4$	8.1514	660, 548, 500
4	$(Fe_{0.496}Mg_{0.498}Ni_{0.001}Mn_{0.009}Ti_{0.002})(Al_{0.458}Cr_{1.305}Fe_{0.227}V_{0.030})O_4$	8.3079	625, 500
5	$(Fe_{0.560}Mg_{0.430}Ni_{0.001}Mn_{0.013}Ti_{0.020})(Al_{0.197}Cr_{1.593}Fe_{0.203}V_{0.003})O_4$	8.3471	618, 495
6	$(Fe_{0.731}Mg_{0.264}Ni_{0.003}Mn_{0.018}Ti_{0.015})(Al_{0.282}Cr_{1.104}Fe_{0.584})O_4$	8.3495	610, 480

Reference:

1. Farmer V.C. Infrared spectra of minerals, London, 1974.

#Rastsvetaeva R.K. Structure and ion-exchange properties of labuntsovite group minerals

Institute of Crystallography RAS, Moscow, Russia E-mail: rast@rsa.crystal.msk.su

At present there is a wide range of natural and thynthetic compounds of labuntsovite family with common chemical formula $A_{10-12}M_8[T_4O_{12}]_4(O,OH)_8 \cdot nH_2O$; A=Ti, Fe, Mn, Mg, Zn, Na, Ca, K, Ba, Sr, Pb, Cs, H_3O; M=Nb, Ti; T=Si, Al, Ga; n~4-16 and cell parameters a=14.18-14.69, b=13.7-14.27, c=7.74-7.93Å, β=117-118° and a=7.35-7.41, b=14.15-14.20, c=7.12-7.15Å. They are of interest due to their zeolite-like frameworks and considerable technological importance as ion-exchange materials [1]. The base of their structures is a mixed framework consisting of the chains of corner-sharing Ti(Nb) octahedra and square rings of Si tetrahedra. In this framework there is a system of channels filled with different A cations and water molecules.

The structures of eight minerals of the labuntsovite group with different chemical compositions have been studied by XRD:
1. Korobitsynite $Na_{8.8}[Ti_{5.6}Nb_{2.4}(O,OH)_8][Si_4O_{12}]_4 \cdot 14.8H_2O$ [2].
2. Lemmleinite $K_{7.2}Na_4[Ti_{5.6}Nb_{2.4}(OH,O)_8][Si_4O_{12}]_4 \cdot 7.2H_2O$ [3].
3. Vuorijarvite $K_6Na_{1.24}[Na_{1.16}(H_2O)_{2.32}][Nb_{4.4}Ti_{3.6}(O,OH)_8][Si_4O_{12}]_{4.6} \cdot 4H_2O$ [4].
4. H_3O-vuorijarvite $(H_3O)_4Na_2K[Sr_{0.4}(H_2O)_{0.8}][Ti_{4.5}Nb_{3.5}(OH_{4.5}O_{3.5})][Si_4O_{12}]_4 \cdot 4H_2O$ [5].
5. Kuzmenkoite $K_{3.2}(H_3O)_{1.5}Na_{0.35}Ba_{0.1}[Mn_{1.4}(H_2O)_{2.8}][(Ti_{3.2}Fe_{0.8})(Ti_{3.6}Nb_{0.4})(OH_{7.6}O_{0.4})][Si_4O_{12}]_4 \cdot 5.7H_2O$ [6].
6. K-labuntsovite (I) $K_{6.8}Na_4[Mn_{0.4}(H_2O)_{0.8}][Ti_{6.4}Nb_{1.6}(O,OH)_8][Si_4O_{12}]_4 \cdot 8H_2O$ [7].
7. K-labuntsovite (II) $K_{5.6}Na_{4.5}Ba_{0.8}[(Mn,Fe)_{0.25}Mg_{0.05}(H_2O)_{0.6}][Ti_{7.2}Nb_{0.8}(O,OH)_8][Si_4O_{12}]_4 \cdot 8H_2O$ [7].
8. Ba-labuntsovite $Na_4K_4Ba_{2.2}[Mn_{0.9}(H_2O)_{1.8}][Ti_8(O,OH)_8][Si_4O_{12}]_4 \cdot 7.2H_2O$ [8].

All the representatives of the family are subdivided into two subgroups - orthorhombic minerals (space group *Pbam*) and monoclinic ones (space groups *C2/m* or *Cm*). In orthorhombic structures the chains are straight while in the monoclinic ones they are screwy and have S-bend.

There is a special position between chains suitable to the additional M(II) octahedron sharing the edges with the chain octahedra.

The orthorhombic minerals are microporous titanium-niobium silicates with the structure of nenadkevichite (korobitsynite) suitable to the substitution of Na atoms by Li and other small ions while the monoclinic representatives are characterized by larger channels of the labuntsovite structure and more appropriate to exchange Na by larger ions and H_3O groups. The structures best suited for ion exchange (lemmleinite type) do not contain any M(II) cations (Ti, Mn, Fe, Mg, Zn ...) which shut some channels.

References:

1. Bortun A.I. et al. *Solvent extraction and ion exchange* (1999) **17** 649.
2. Rastsvetaeva R.K., Chukanov N.V., Pekov I.V. *Dokl. Ross. Akad. Nauk* (1997) **357** 364.
3. Rastsvetaeva R.K., Arakcheeva A.V., Khomyakov A.P. *Dokl. Ross. Akad. Nauk* (1996) **351** 207.
4. Rastsvetaeva R.K. et al. *Eur. Miner.* (1994) **6** 503.
5. Rastsvetaeva R.K. et al. *Dokl. Ross. Akad. Nauk* (2000) (in press).
6. Rastsvetaeva R.K., Chukanov N.V., Pekov I.V. *Crystallogr. Reports* (2000) (in press).
7. Rastsvetaeva R.K. et al. *Crystallogr. Reports* (1998) **43** 874.
8. Rastsvetaeva R.K., Chukanov N.V., Pekov I.V. *Dokl. Ross. Akad. Nauk* (1997) **357** 64.

Kiseleva I.A[1], Ogorodova L.P.[1], Melchakova L.V.[1], Getmanskya T.I.[2] Thermodynamic properties of creedite Ca$_3$Al$_2$(F,OH)$_{10}$(SO$_4$)$\cdot$2H$_2$O

[1] Department of Geology, Moscow State University, Vorobyevy Gory, Moscow 119899, Russia
[2] Vserossiiski Institute of Mineral Raw Materials, Staromonetny per., 3 Moscow 109017, Russia; mineral@geol.msu.ru

key words: [*creedite, calorimetry, heat capacity, enthalpy and Gibbs free energy of formation*]

Creedite – complicated fluoride - $Ca_3Al_2(F,OH)_{10}(SO_4) \cdot 2H_2O$, was first found in Colorado (USA), and subsequently repeatedly described in oxidized zones and ore formations of Mo-W deposits of Central Kazakhstan [1,2]. Creedite was investigated by chemical, X-ray diffraction, optical and thermal methods [1-3]. There are no data on thermodynamic properties of creedite. The present work uses the different calorimetric methods to measure the heat capacity, the enthalpies of

formation of mineral. The first data on standard thermodynamic properties of natural creedite , such as heat capacity, enthalpy of formation, entropy and free Gibbs energy are given.

We chose for investigation well crystallized transparent crystals of creedite (Akchatau, Kazakhstan) from aggreation and druses of late stages of hydrothermal process. Creedite was analyzed by microchemical method. The composition of creedite is very close to the theoretical one. Crystallochemical formula of creedite was calculated for 5 cations: - $Ca_3Al_2F_{8.25}(OH)_{1.75}(SO_4) \cdot 2H_2O$. The relation F/OH in the mineral is higher, than in all compositions investigated earlier. X-ray study of creedite confirmed the monoclinic symmetry. Lattice parameters of creedite studied agree well with the previous literature data [3].

High-temperature thermal behavior was studied using the methods of differential thermal (DTA) and thermogravimetric (TG, DTG) analyses and differential scanning calorimetry (DSC). It is characterized by two legiblly expressed endothermic processes. First of them occurs at 430-450 ^{o}C and corresponds to losses of water and hydroxyl group (about 11 %). As shown by DSC measurement the process of dehydration is accompanied by endothermic effect 220.3±4.1 kJ/mol. The second endoeffect with a maximum at 815 ^{o}C is produced by the reversible phase transition of decomposition products of creedite. Exoeffects at temperatures about 540°C and 730°C are minor. The composition of products of heating up to 1400 ^{o}C is very multiphase, losses of mass reach 32 %.

The thermochemical investigations were performed in differential scanning calorimeter DSC «Mettler TA-2000B» and high-temperature heat-flux Calvet microcalorimeter «Setaram».

The heat capacity of creedite was measured by DSC method in the interval of 280-610 K in flowing nitrogen with a heating rate of 5-10 K/min. The molar enthalpy and melting temperature of indium reference substance (99.9999 % purity) were used to calibrate the DSC. The DSC measurement results in the interval of 280-610 K were fitted by least-squares yielding with respective average deviation of approximation presented in brackets:
$C^{o}p = 423.80 + 379.45 \cdot 10^{-3}T – 88.70 \cdot 10^{5}T^{-2}$ J/mol·K ($\pm \pm 1,3\%$) at 298.15-610 K

Enthalpy of formation of creedite was determined by a set of thermochemical cycles using decomposition at 717 K (temperature of dehydration) and subsequent dissolution of decomposition products in molten lead borate, both reactions taking place in a Calvet calorimeter. The transposed temperature drop calorimetry method (sample was dropped into a calorimeter at 717 K) was used to obtain enthalpies of dehydration reaction. When sample was dropped into a calorimeter at 717 K the heat effect measured was thus the sum of the heat content and the enthalpy of dehydrated at 717 K creedite - $[(H^{o}_{717}-H^{o}_{298.15})+\Delta H^{o}_{dehyd \cdot 717}]$. When the dehydrated creedite was dropped into the calorimeter and only heated from T=298.15 to T=717 K, the heat effect ($H^{o}_{717}-H^{o}_{298.15}$) was measured . The heat of dehydration was calculated from the experimental data.

The transposed temperature drop solution calorimetry method was used to obtain the enthalpy of solution of the dehydrated creedite. Samples of dehydrated creedite were dropped into molten $2PBO \cdot B_2O_3$ held at T=973 K. The heat effect measured was the sum of the heat content and the enthalpy of solution of the dehydrated creedite - $[(H^{o}_{973}-H^{o}_{298.15})+ \Delta H^{o}_{sol.973}]$.

Calibration was performed by the Pt and α-Al_2O_3 drop method. A precision of weighing the samples was $\pm 2 \cdot 10^{-3}$ mg.

Table 1. Results of the calorimetric study of creedite (F.W.=492.787)

Mineral	Observed values	kJ/mol
Creedite	$[(H^{o}_{717}-H^{o}_{298.15})+\Delta H^{o}_{dehyd \cdot 717}]$	458.8 ± 3.7 (7)
Dehydrated creedite	$(H^{o}_{717}-H^{o}_{298.15})$	185.4 ± 0.8 (12)
Dehydrated creedite	$[(H^{o}_{973}-H^{o}_{298.15})+\Delta H^{o}_{sol.973}]$	498.8 ± 5.2 (10)

The standard enthalpy of formation of creedite from elements were calculated using the experimental values of table 1 as a sum of the enthalpy of dehydration and the enthalpy of formation of dehydrated creedite from the constituent substances such as CaO, $CaSO_4$, CaF_2 and AlF_3.

The entropy of creedite was estimated by addition of the entropies of the constituent cations and anions using Latimer method. By combining our data on the enthalpy of formation with the entropy values we estimated the standard molar Gibbs free energy of formation of creedite at 298.15 K(table 2). The thermodynamic data produced by this study can be useful for understanding creedite stability in low-temperature complex natural systems.

Table 2. Thermodynamic properties of creedite $Ca_3Al_2F_{8.25}(OH)_{1.75}(SO_4) \cdot 2H_2O$ (F.W.=492.787) at 298.15 K

V^{o}cm^3	S^{o} ,J/mol·K	ΔH^{o}_f ,kJ/mol	ΔG^{o}_f,kJ/mol	C$^{o}_p$ J/mol·K
178,0	501[1]	-7379.6 ± 1.2	-6866	437.2

[1] – estimation by Latimer method

References:

1. Yermilova L.P., Moleva V.A. Doklady Akademii nayk SSSR, 1953, 88, 5, 905
2. Miroshnichenko A.B. Izvestia Kaz. Ak.nayk., 1955,119,199
3. Borisov S B., Brusentsov F.A., Klevtzov R.F., Belov N.I. Doklady Akademii nayk SSSR, 1964, 155, 6, 1082

Rosenberg[1] К.A, Sobolev[2] A.V. Mossbauer spectroscopy and X-ray study of chrysolites of various origin

[1]Moscow State University, geological department, Vorobjovy Gory, Moscow, 119899, Russia;
[2]Moscow State University, chemical department, Vorobjovy Gory, Moscow, 119899, Russia
mineral@geol.msu.ru

Chrysolite - a gem quality magnesium olivine - taken out of various deposits in the world has been studied in this work by the methods of Mossbauer spectroscopy, X-ray and microprobe analysis. Structural and chemical composition features have been examined for chrysolites of various origin including igneous chrysolite embedded in olivine basalts (Arizona, USA) and in alkali basalts (Hawaii); chrysolite from the xenolites in kimberlites (pipe Udachnaya and pipe Obnagonnaya in Yakutia) and metamorthic chrysolite from the serpentine veins in peridotites (Nuristan, Pakistan) and from veins among olivinites in hyperbasites (Kugda, East Siberia).

The microprobe analysis of chrysolites had been done with the electron microprobe Camebax SX-50. Powder X-ray diffraction was carried out with DRON-UM1 diffractometer using Co k_α radiation. Data were collected in a step scan mode using step of 0.05^o with counting time of 2s. Metallic Si was used as internal standard for determination of the unit cell parameters.

Mossbauer spectra measurements were made using electrodynamic motor spectrometer, working in a constant acceleration mode. Spectra were received on ^{57}Fe nuclei in olivines studied as absorbents of resonant γ-rays using the ^{57}Co(Rh) source. Mossbauer spectra were approximized by combination of resonance lines, having Lourence shape in the case of thin layer of the sample. The least square method was used for approximation. The work on spectra was done with the «Mossbauer Calculation System» computer program.

The results of microprobe and X-Ray analysis are represented in table 1.

Table 1.

N	Occurrence, Locality	Colour	% Fa	Unit cell parameters, Å		
				a	b	c
1	Olivine basalts (Arizona, USA)	olive-green	11	4.727(3)	10.240(5)	5.994(3)
2	Alkali basalts (Hawaii)	olive-green	15	4.764(5)	10.206(5)	5.985 (4)
3		brown	21	4.767(5)	10.237(7)	6.0004(5)
4	Kimberlites (pipe Udachnaya, Yakutia)	light green	7	4.727(3)	10.161(3)	5.964(3)
5		olive	7.5	4.748(3)	10.204(5)	5.982(2)
6		brown	13.5	4.760(2)	10.220(4)	5.985(2)
7	Kimberlites (pipe Obnagonnaya, Yakutia)	olive-green	7.3	4.745(4)	10.201(5)	5.988(4)
8		gr.-brown	11.5	4.724(4)	10.236(5)	5.999(4)
9	Veins among olivinites in hyperbasites (Kugda, East Siberia).	green	11	4.784(3)	10.139(5)	5.929(2)
10	Serpentine veins in peridotites (Nuristan, Pakistan)	light green	6.5	4.722(4)	10.197(5)	5.974(4)

The amount of Fa in analyzed samples (22) ranges from 5-6 to 21 mol.%. Chrysolites from basalts have the highest amount of iron (11-21 mol.% Fa). The composition of gem quality chrysolites from Udachnaya pipe were studied in more detail for each color group (there are 8 color groups ranging from light green to dark brown). In seven color groups iron contant is almost the same (7-8 mol.%Fa), while dark brown samples content up to 13.5mol.% Fa. There is a trend to iron contain increase as the color change from light green to brown.

Impurities content (MnO, Cr_2O_3, TiO_2) is not high in chrysolites studied except for NiO content. NiO impurity (0.20-0.55 mas.%) is detected in all samples. In samples № 2, 3, 9 some content of MnO (0.22-0.51mas.%) and CaO (0.20-0.34 mas.%) were found.

The determined lattice parameters of chrysolite are of quite close values and have a trend to increase as iron content grows up.

The Mossbauer spectra of chysolites, measured on ^{57}Fe nuclei at 295K, consist of a single asymmetric quadropole doublet, which represents a superposition of two doublets. These two doublets correspond for Fe^{2+} in two nonequivalent cation positions – M1 (local symmetry D_{4h}) and M2 (local symmetry C_{3v}). The value of isomer shifts, for the Fe^{2+} in D_{4h} and C_{3v} positions account to high spin configuration of Fe^{2+} (table 2) . Such configuration is common for Fe^{2+} - oxygen compounds. A big value of quadrupole splitting for Fe^{2+} in olivine is caused, for the main part, by asymmetry of electron surrounding of Fe^{2+} ions (d^6 configuration). The distribution of Fe^{2+} between M1 and M2 sites showed no ordering it is statistics, and makes the doublets in spectra get wide.

Table 2. Mossbauer spectra parameters for Fe^{2+} in olivines

Sample	isomer shift, mm/s		Quadrupole splitting, mm/s		Position distribution,%	
	M1	M2	M1	M2	M1	M2
4	1.34	1.15	3.05	3.03	50.01	49.99

5	1.34	1.12	3.10	3.09	51.87	48.13
6	1.32	1.21	3.15	3.12	53.11	46.89
1	1.27	1.11	3.00	2.99	47.56	49.53
9	1.24	1.11	3.00	2.97	50.20	49.80
10	1.33	1.23	3.17	3.11	49.21	44.54

In Mossbauer spectra of metamorphic chrysolites (samples 9,10), besides a wide Fe^{2+} doublet, a small absorption area in the center was found (its parameters are: $\delta = 0.32 - 0.35$ mm/s). We assume this area accounts for Fe^{3+} (d^5 configuration) occupancy of cation positions in olivine structure. The value of electrical field gradient ($\Delta = 0.55 - 0.57$ mm/s) on Fe^{3+} nuclei is caused by the distortion of octahedral oxygen surrounding. The content of Fe^{3+} in chrysolite from Kugda (sample №9) is 2,8% out of total iron content in this sample. The content of Fe^{3+} in chrysolite from Pakistan (sample №10) is 6.3% out of total iron content.

Despite of the small Fe^{3+} doublet area, the error of Fe^{3+} content determination is less than 0.8%.

The study showed differences in chemical composition of chrysolites of various origin. Igneous chrysolites have insignificant or do not have at all any Fe^{+3} ions in cation positions in the structure. This conforms to geological views of high temperature and high pressure olivine crystallization at the reduction conditions. Metamorphic chrysolite studied formed in serpentine veins among olivinites in hyperbasites according to Mossbauer study data have a steady significant content of Fe^{3+} ions. This fact indicates that metamorphic chrysolites are formed as the result of serpentine dehydration at high oxidation conditions in low depth.

[#]SuvorovaV.A., Kotelnikov A.R. Synthetic titanates (synthesis and properties).

key words: [*titanates, synthesis, chemical and physical properties, parameters of the elementary cell*]

The purpose of this work was to study properties and determine parameters of the elementary cell of synthesized accesory minerals (perovskite, loparite) as well as Eu aluminate. As a rule, these compounds are solid solutions and potential matrices to fix alkaline, alkaline- and rare-earth elements (Cs, Sr, Ba, Ce, Eu etc) which can enter the crystalline lattice of minerals as isomorphous impurities, replacing Ca-atoms and partially Ti. A well-known stability of these minerals at airing of rocks, gives us grounds to expect their stability and radionuclide leaching.

Mineral synthesis was made by hot pressing method in 3 stages: 1) drying of charge in vacuum during 0.5 hour; 2) pressing at 1350^0C and axis pressure of 300 bar during 0.5 hour; 3) completing synthesis at 1350^0C and remaining axis pressure (50 bar) during 4 hours [1]. Synthesized solid solution of titanates which Na, Ca, Sr, Ce and Eu enter isomorphously, represent samples of poly- and monomineral ceramics with the density of 88-98% from the theoretical one. Chemical composition, equations of synthesized matrices and stable phases of the studied part of the system CaO - (SrO) - (EuO) - TiO - CeO_2 are given in Tabl.1 (according to microprobe data).

Table 1. Contens of oxides (wt%) and formulas of samples.

N sample	Mineral phase	CaO	SrO	TiO$_2$	Ce$_2$O$_3$	Formula
1104/1	Prv[a]	48.24	-	51.76	-	$Ca_{1.98}Ti_{2.02}O_{6.02}$
1105/1	SrPrv[b]	23.41	6.13	55.46	-	$(Ca_{0.82}Sr_{0.18})_{1.98}Ti_{2.02}O_{6.02}$
1108/1	Lpr[c]	Na$_2$O 22.55	-	54.17	21.21	$Na_{0.8}Ce_{1.18}Ti_{2.00}O_{6.2}$
1109/1	EuLpr[d]	Na$_2$O 22.55	Eu$_2$O$_3$ 2.066	54.17	21.21	$Na_{0.91}(Ce_{0.91}Eu_{0.09})_{1.08}Ti_{2.07}O_{6.1}$
1113/1	Sr Prd[e]	K$_2$O 2.27	9.39	65.17	MgO 12.89	$(K_{0.4}Sr_{0.8})_{1.2}Mg_{0.2}Ti_{6.8}O_{16}$
Cт 20/2	EuAlO$_3$	BaO 1.73	Eu$_2$O$_3$ 73.5	Al$_2$O$_3$ 19.18	SiO$_2$ 2.33	$(Eu_{1.03}Gd_{0.02}Ca_{0.01}Ba_{0.01}Fe_{0.027}Si_{0.084})_{1.2}Al_{0.8}O_3$

Note: [a] - perovskite; [b] - Sr-bearing perovskite; [c] - loparite; [d] - Eu- bearing loparite; [e] - Sr- bearing priderite

Table 2. Parameters of the elementary cell of the number of the titanates row and Eu aluminate.

N sample	Basic phase	Structure[*]	a, E	b, E	c, E	α, °	β, °	γ, °	V, (E)^3
1104/1	Prv	orto [2]	5.382	7.646	5.446	90.00	90.00	90.00	224.2

			(08)	(1)	(07)				(0.4)
1105/1	Sr Prv	«	5.420 (3)	7.757 (7)	5.436 (2)	90.00	90.00	90.00	225.6 (2)
1109/1	EuLpr	«	5.769 (14)	7.723 (16)	5.454 (12)	90.00	90.00	90.00	242.9 (7)
Cт 20/2	EuAlO$_3$	orto [3]	5.273 (2)	5.291 (2)	7.467 (2)	90.03 (1)	90.46 (1)	89.76 (1)	208.3 (0.7)

Note: * - structure in the approximation of which the calculation was made.

These samples of titanates and aluminate were tested on leaching of Na, Sr, and Ca.

Table 3. Velocities V(g/m^2/day) of leaching Na from the ceramic matrix consisting of the titanates as compared with natural plagioclase.

Mineral phase	Density, g/sm^3	Wt% Na of initial sample	0-1 days	1-7 days	7-14 days	7-28 days	References
Pl*	2.67	4.91	1.55	0.09	0.03	0.004	[4]
Lpr	4.78	6.10	2.76	3.45 ·10^{-2}	6.27 ·10^{-3}	5.87 ·10^{-3}	This work 1108/1
EuLpr	4.29	6.50	1.00	5.78 ·10^{-2}	2.10 ·10^{-2}	9.83 ·10^{-3}	This work 1109/1
EuLpr	4.29	6.50	1.23	1.5 ·10^{-2}	-	1.7 ·10^{-2}	This work 1109/2**

Note: * - natural plagioclase;
** - after the annealing in muffle furnace at 1240°C during 2 days.

Table 4. Velocities V(g/m^2/day) of leaching Ca from the natural minerals, ceramic matrix of the Synroc type and synthetic zirconates.

Mineral phase	Density, g/sm^3	Wt% Ca of initial sample	0-1 days	1-7 days	7-14 days	7-28 days	References
Pl	2.67	7.75	0.630	0.090	0.043	0.013	[4]
Synrock-C	~4.5	6.70	-	0.003	-	0.006	[5]
(Ca,Sr)TiO$_3$ - SrPrv	4.41	22.0	0.366	0.110	0.022	0.011	This work №1123/1
(Ca,Sr)Ti$_3$O$_7$ - SrPrv + Rt*	3.67	7.63	0.547	0.068	0.025	0.012	This work №1127/1

Note: * - rutile.

Table 5. Velocities V(g/m^2/day) of leaching Sr from ceramic matrix of the Synroc type and synthetic titanates.

Mineral phase	Density, g/sm^3	Wt% Sr of initial sample	0-1 days	1-7 days	7-14 days	7-28 days	References
Synrock C	~4.5	0.41	-	0.007	-	0.010	[5]
(K,Sr)MgTi$_7$O$_{16}$ - SrPrd	3.39	9.99	6.44	1.420	-	0.400	This work №1113/1
(Ca,Sr)TiO$_3$ - SrPrv	4.41	12.3	1.01	0.269	0.07	0.033	This work №1123/1
(Ca,Sr)Ti$_3$O$_7$ - SrPrv + Rt	3.67	11.12	1.31	0.640	0.06	0.028	This work №1127/1

Table 6. Velocities $V(g/m^2/day)$ of leaching Ce from the ceramic matrix of the Synroc type, of the NZP type, phosphate matrices and synthetic titanates.

Mineral phase	Den-sity, g/sm^3	Wt% Ce of initial sample	0-1 days	1-7 days	7-28 days	References
Synrock C	~4.5	1.93	-	$6×10^{-6}$	$1×10^{-5}$	[5]
$NZP+Mz^a+ZP^b+ CsZP^c$	3.23	2.57	-	0.0008	$5×10^{-5}$	[6]
$CePO_4 + Alt^d$	2.74	21.70	0.0004	0.00005	$2×10^{-5}$	[7]
$CePO_4 + Avg^e$	2.79	23.29	0.0003	0.0002	$3×10^{-5}$	[7]
$Na(Ce,Eu)Ti_2O_6$ EuLpr	5.48	47.25	0.0008	0.00001	$5×10^{-6}$	This work №1109/2

Note: [a] - monazite; [b] - ZrP_2O_7; [c] - Cs-bearing ZrP_2O_7; [d] - allanite $(Na,Ca,Ce)_2(Al,Fe)_3Si_3O_{12}[O,OH]$; [e] - avgite $(Na,Ca,Ce)(Mg,Fe,Al)[(Si, Al)_2O_6]$.

Table 7. Velocities $V(g/m^2/day)$ of Eu-leaching from the ceramic matrix consiting of titanates and aluminates.

Mineral phase	Den-sity, g/sm^3	Wt% Eu of initial sample	0-1 days	1-7 days	7-28 days	N sample
$Na(Ce,Eu)Ti_2O_6$ - EuLpr	5.48	2.29	0.00076	0.000014	0.000009	1109/2
$EuAlO_3$	5.60	63.21	0.00048	0.0003	0.00011	Ст20/2

The given data on the leaching of Ce and Eu testify to the uniqueness of titanates as matrices, keeping these elements. For some of these solid solution parameters of the elementary (PEC) cell are calculated. The results of the calculations are given in Tabl.2 (the errors of some more exact definitions are given in brackets and refer to the last decimal signs).

One should emphasize that velocities of leaching V $g/(m^2·day)$ of alkaline and alkaline-earth elements from solid solution of titanates increase in the following sequence: Na -> Ca -> Sr. Low velocities of leaching Na, Ca, Sr and Ti (no leaching from any sample) showed high stability of solid solutions of loparite and perovskite, constituting synthesized samples, comparable with the stability of Sinrok-C [4] and natural monocrystals of plagioclase [5]. It testifies to a possibility to use these solid solutions of titanates as matrix materials - fixators of alkaline, alkaline- and rare-earth radionuclides of RAW (radioactive waste).

Moreover, the samples of titanates and aluminate were subjected by us to leaching of Ce and Eu from them. The results are shown in Tabl.6 and 7.

References:

1. Martinov K.V. et al. Synthesis and study of the composition and properties of ceramic matrices on the basis of minerals of complex oxide group bearing elements-imitators of RAW // 4th Annual Scientific & Technical Conference of the Nuclear Society «Nuclear Energy and Man Security NE-93» June 28- Jule 2, 1993, Nizhni Novgorod, Abs. of Conf, part.II, pp.968 - 969 (in Russian).
2. Chichagov, A.V. et al. Information-Calculation System on Crystal Structure Data of Minerals (MINCRYST) // Kristallografiya, v.35, n.3,1990, pp.610-616 (in Russian).
3. PDF, N 9-84.
4. Kotelnikov A.R., Akhmedzhanova G.M. and Suvorova V.A. Minerals and their solid solution - matrices for immobilization of radioactive waste // Geochemistry, 1999, № 2, pp.1-9, (in Russian).
5. Ringwood A.E. et al. SYNROC. In: Radioactive waste forms for future (eds. Lutze and Ewing).1988, ch.4, pp.232-334.

[#]**Shchapova Yu.[1], Votyakov S.[2], Yuryeva E.[3], Ivanovskii A.[3] Peculiarities of chemical bond metal-ligand and effects of non-statistic cation distribution in chrom-spinelides (results of quantochemical modeling)**

[1] Ural State Technical University

[2] Institute of Geology and Geochemistry, Ural Branch RAS

[3] Institute of Solid-State Chemistry, Ural Branch RAS votyakov@igg.uran.ru

key words: [*chemical bond, electronic structure, spinel, cation distribution, Mossbauer spectroscopy*]

Standard recalculations of crystallochemical formulae of minerals, which is a basis for petrological and geochemical studies, considers an ionic character of a metal-ligand bond. However, that is mostly a model. An absence of an alternative approach, as well as calculations and experimental data on the degree of covalent bonding in minerals is responsible for the appearance of internally conflicting results. The present study shows the results of the investigation of peculiarities of electronic structure and chemical bonds of iron ions in crystalline matrix with possible deviations of cation distribution in tetrahedral position from equally probable, exemplified by chromium spinel $(Mg_x,Fe_{IV(1-x)})(Cr,Al,Fe_{VI})_2O_4$ of normal structure [I]. The mineral was chosen as an object for study, since it

is commonly used in oxybarometers [1] for quantitative estimations of oxidation state in the upper mantle. However, using the stoichiometric model for spinel composition, based on the ionic character of bonds, results in inconsistencies of three or four orders of magnitude in the estimations of oxygen fugacity. We carried out the quantochemical modeling of electronic structure of chromium spinel using the non-empirical cluster method of X_α-discrete variation. The details of the calculations are discussed in [2-4]. Samples of intermediate composition were modeled by fragments of structure, containing a central iron-oxygen octahedron $Fe_{VI}O_6$ (or $Cr_{VI}O_6$ and $Al_{VI}O_6$ octahedrons), surrounded by six tetrahedrons $Mg_{IV}O_4$ and $Fe_{IV}O_4$. Variations of mineral Fe-number (x = 0÷1) were fixed by number of cations Mg_{IV} and Fe_{IV}. In order to simplify the calculations, an influence of cations Fe_{VI}, Cr_{VI}, and Al_{VI}, neighboring in a real structure with the central octahedron, was not regarded. The correctness of the structural model was estimated on the basis of comparison of calculated parameters of the nuclear gamma-resonance spectra with the experimental ones.

The calculations adequately reproduce the basic features of electronic structure of complex iron oxides, including the relative position of $Fe_{VI}3d$ and $O2s,2p$ valent levels in a spectrum, the splitting of 3d-levels in crystalline field, and their spin polarization [2]. A partial overlap by energies of valent states of oxygen and iron, as well as their notable covalent mixing, are observed for all the studied compositions, values of occupancies of superposition of $Fe_{VI}3d,4s,4p$ and $02s,2p$ orbitals, which can be used as an indicator of degree of covalent bonding, are not non-zero. The largest covalent effect is observed for $O2p$- and $Fe_{VI}3d,3s$ orbitals. The calculations indicated, that the bond metal-ligand was more ionic for oxygen in the coordination Fe_{VI}-O-Mg_{IV} as compared to oxygen in the Fe_{VI}-O-Fe_{IV} coordination. The degree of ionic bonding is found to increase with replacement of Fe_{IV} by Mg_{IV} in tetrahedron site of the structure around Fe_{VI} ion. Values of Q, i.e. the effective ion charge, for Fe_{VI} (+ 1.64 - 1.76), Mg_{VI} (+ 1.22), Fe_{VI} (+ 1.00), Cr_{VI} (+ 1.80), Al_{VI} (+ 2.17), and oxygen (-1.17 ÷ -1.47), calculated by the method [5], appreciably differ from whole number values, commonly used in mineral crystal chemistry. Charges of oxygen ions are found to significantly vary, depending on the nearest cation surrounding. The largest charge of oxygen ions is observed in the Al_{VI}-O-Mg_{IV} coordination, the smallest charge is observed in the Fe_{VI}-O-Fe_{IV} coordination. That supports the conclusion about more covalent character of bonding in the second case. The effective charge of Fe_{VI} ions increases with decrease of Fe-number (increase of x value). The increase of the degree of ionic bonding in the Fe_{VI}-O-Mg_{IV} bond is reflected in the increase of effective charge of the above type of oxygen.

On the basis of the obtained effective charges and data on chemical analyses and nuclear gamma-resonance, we carried out calculations of positive and negative charges of cationic and anionic sub-lattices of the samples [3J. We found, that in the frames of the above assumptions about the normal distribution of cations and stoicheometry of oxygen, the condition of electro neutrality of the lattice could be valid only at the existence of preferential coordination of oxygen ions, which promote a negative charge of the anionic sub-lattice. This condition implies deviation of

cation distribution in the spinel structure from equally probable and formation of cation associates. The study of the number of chromium spinel probes collected from Ural ultrabasic rocks showed, that the highest inhomogeneity was observed in Fe-rich samples. That quantitatively agrees with experimental micro-x-ray spectral data, which indicate, that Fe-rich chromites are characterized by inhomogeneity in distribution of iron and magnesium within grains,

Asymmetry of distribution of electronic density of 3d-orbitals of Fe_{IV} ions and charge non-equality of nearest atoms of oxygen lead to formation of similar by order of value of electron and lattice contributions into gradient of electrostatic field on iron core and value of quadrupole splitting (QS) of the nuclear gamma-resonance spectra [4], According to the calculations, dependence of QS on composition of the samples is not additive, the maximal resulting value QS (0.3 - 05 mm/sec) is reached for Fe_{IV} ions, whose local surrounding corresponds to x = 0.17 - 0.33. It can be assumed, that the observed experimental tendency of an increase of QS with a decrease of Fe- number [1] is related to formation of cationic associates of such composition in the region of intermediate iron concentrations. At the same time, the formation of the electric field gradient on the iron core must be greatly influenced by such local structural factors, as distortions of iron-oxygen octahedrons, presence of vacancies, and so far. Therefore, an interpretation of the nuclear gamma-resonance parameters calls for further investigation.

Thus, chemical bond metal-ligand in chromium spinel is significantly covalent, and is defined by local surrounding of oxygen octahedron. Crystallochemical description of samples accounting of peculiarities of their electronic structure and chemical bond needs an admittance of deviation of cationic distribution from the equally probable and formation of the cationic associates. Suggestion about non-statistical cationic distribution agrees with the results of experimental and theoretical analysis of the nuclear gamma-resonance spectra.

References:

1. Chashchukhin I.S., Votyakov S.L., Uimin S.G., BorisovD.R.., Bykov V.N. Nuclear gamma-resonance spectrography of chromium spinels and problems of oxythermobarometry of chromite-bearing Ural ultrabasic rocks. Ekaterinburg, Nauka, 1996, 136 p.
2. Blinov '3.S., Shchapova Yu.V., Yur'eva E.T., Ryzhkov M.V., Ivanovskii A.L., Votyakov S.L. Influence of composition and structure of the second coordination sphere on electronic structure and parameters of the nuclear gamma-resonance of Fe^{3+} ions in complex oxides. In: Problems of spectroscopy and spectrometry. Interinstitution scientific transaction, Ekaterinburg, Ural Technical State University, !999, issue 2, pp.34-41.
3. Votyakov S.L, Shchapova Yu.V., Chashchukhin I.S., Yur'eva E.I., Ryzhkov M.V,, Ivanovskii A.L. On the degree of covalent bonding of the metal-ligand bond in chromium spinel (data of quantochemical calculations). Annual book of the Institute of Geology and Geochemistry of Ural Branch RAS, Ekaterinburg, Publishing House of Ural Branch RAS, 2000 (in press).

4. Shchapova Yu.V., E.I, Yur'eva, S.L. Votyakov, A.L. Ivanovskii. Electronic structure and parameters of the nuclear gamma-resonance spectra of Fe^{3+} ions in chromium spinels, non-empirical quantochemical calculations. Annual book of the Institute of Geology and Geochemistry of Ural Branch RAS, Ekaterinburg, Publishing House of Ural Branch RAS, 1999, pp. 182-189.

5. Ryzhkov M.V. New approach to calculation of effective charges of atoms in Molecules, clusters, and solids, Journal of Structural Chemistry, 1998, v. 39, no. 6, pp. 1134-1140.

Kotelnikov A.R. [1], Kovalsky A.M. [1], Trubach I.G., [2] Orlova A.I., [2] Petkov V.I.[3] Synthesis and X-ray study of solid solutions $(Ca,Sr)_{0.5}Zr_2(PO_4)_3$.

[1] Institute of Experimental Mineralogy of Russian Academy of Sciences, Chernogolovka, Moscow distr., 142432,
[2] Chemical department, Nizhniy Novgorod State University Gagarina str., 23, Nizhniy Novgorod,603600,

key words: [*zirconium-phosphates, solid solutions, experimental study*]

Introduction. Calcium-strontium zirconium-phosphates form the orthophosphate group are characterized by the wide development of isomorphic replacement of various groups of elements [1]. The general formula of the orthophosphate group is:
$(AxIByIIRzIIIMvIVCwV)(XO4)n$, where n = 1,2,3,4...., and x, y, z, v, w can accept both whole, and fractional meanings, and also zero.
(A) - one - valence elements - H, Li, Na, K, Rb, Cs, Cu, Ag, Tl;
(B) - two- valence elements - Be, Ca, Sr, Ba, Cu, Cd, Pb, Mn, Fe, Co, Ni, Eu;
(R) - three- valence elements - Sc, Y, La, Al, Ga, In, Bi, Cr, Fe, Co, Ce-Lu, Pu-Cm;
(M) - four- valence elements - Ti, Zr, Hf, Ge, Sn, Ce, Th, U, Np, Pu;
(C) - five- valence elements - Nb, Ta, Sb.
X - P, As, V.

Zirconium- phosphate solid solutions are of interest for the study of thermodynamics of isomorphic replacements in various positions (within the framework of one structure). Besides, zirconium- phosphate solid solutions are perspective matrix material for radioactive waste elements immobilization, that is determined both by wide development of isomorphic replacements, and high stability of these solid solutions to leaching processes. The aim of our work was the experimental study of isomorphic replacements of Ca and Sr in zirconium- phosphate solid solutions: $(Ca, Sr)_{0.5}Zr_2(PO_4)_3$.

Experimental study of solid solutions $(Ca, Sr)_{0.5}Zr_2(PO_4)_3$

Starting materials. The mechanical mixtures of $Ca_{0.5}Zr_2(PO_4)_3$ and $Sr_{0.5}Zr_2(PO_4)_3$, prepared by a zol-gel method and synthered at 800-1000°C during 1-3 days. On the basis of X-ray study data zirconium- phosphates corresponded to described in PDF JCPDS zirconium- phosphate solid solutions (space group R3c, Z = 6).

Experimental technique and procedure. The runs were carried out in the welded platinum ampoules which were placed into high pressure hydrothermal cold seal vessels with external heating. 80-100 mg starting materials (mixtures of $Ca_{0.5}Zr_2(PO_4)_3$ and $Sr_{0.5}Zr_2(PO_4)_3$) were loaded into capsules, necessary amount of distilled water was added. In each run solid reagents were represented by $Ca_{0.5}Zr_2(PO_4)_3$ and $Sr_{0.5}Zr_2(PO_4)_3$ mixtures, taken in various ratios. The experiments were carried out at 750°C and water pressure of 2 kbar. The accuracy of temperature control was not worse than 5°C, pressure control was not worse than 50bars. The run duration was 15-20 days.

Analytical methods. X-ray study of zirconium- phosphate solid solutions was carried out using the powder diffractometer HZG-4 in the mode of constant scanning. Si of spectral purity was used as the internal standard. Calculation of the unit cell parameters was carried out till 12-17 reflections within the angle range 7-39°(Θ). Cell parameters refinement was carried out using of the programs LCC, PUDI [2], REFLAT [3].

Microprobe analysis was carried out on the device "Camebax" with energydispersive detector Link AN-10000; the method of ZAF-correction was used for the determination of the composition of zirconium- phosphate solid solutions. The accuracy of microprobe analysis of solid solution composition was 2.5 mol.%.

Results of experiments. As shown by the analysis of the solid products of experiments, (Ca, Sr) - zirconium-phosphate solid solutions form a continuous series of solid solutions at 750°C and P=2kbar. The variations of grains compositions in one experiment do not exceed 3-4 mol.%. The investigated phases of zirconium- phosphate solid solutions from the data of X-ray study form a series of structural analogues described in space group. R3c. The results of cell parameters refinement of zirconium- phosphate solid solutions are listed in Table 1.

Table 1. Unit cell parameters of (Ca, Sr)- of zirconium- phosphate solid solutions.

X_{Sr}	a, [A]	c, [A]	V, [A]^3	Reference
0.0	8.772(2)$^{1)}$	22.766(6)	1517.2(4)	1
0.0	8.772(1)	22.759(4)	1516.9(3)	1
0.12(3)	8.757(1)	22.881(5)	1519.9(4)	1
0.24(2)	8.744(2)	23.034(5)	1525.1(5)	1
0.64(3)	8.722(1)	23.149(6)	1525.0(6)	1
0.93(4)	8.696(1)	23.315(5)	1526.9(3)	1
1.00	8.700(1)	23.330(4)	1529.9(3)	1
0.0	8.785	22.680	1516.1	2
1.0	8.693	23.380	1530.8	2

1) The standard errors of calculation are given in brackets and refer to last decimal place. Reference: 1 - this work; 2 - PDF JCPDS data.

The concentration dependences of the unit cell parameters of the solid solutions $(Ca, Sr)_{0.5}Zr_2(PO_4)_3$ are characterized by nonlinear curves and can be described by the following equations of the 3-rd order:

$a = 8.7723 - 0.13776 \cdot X + 0.129335 \cdot X^2 - 0.067508 \cdot X^3$ [A] (± 0.003) (1)

$c = 22.757 + 1.45150 \cdot X - 2.00305 \cdot X^2 + 1.139735 \cdot X^3$ [A] (± 0.021) (2)

$V = 1516.75 + 49.24236 \cdot X - 93.24639 \cdot X^2 + 56.7028 \cdot X^3$ [A]^3 (± 0.9) (3)

where X - mole fraction of Sr in solid solution of (Ca, Sr)-zirconium- phosphate. On the basis of the equations (1) - (3) excess volume of solid solutions $(Ca, Sr)_{0.5}Zr_2(PO_4)_3$ was calculated. The compositional dependence of excess volume was approximated by the following equation:

$V^e = -0.008544 + 36.567 \cdot X - 95.4772 \cdot X^2 + 58.8625 \cdot X^3$ [A^3/mole] (± 0.6) (4)

The excess functions of solid solutions are convenient for describing within the framework of Margules model: $F^e = X_1 \cdot X_2 \cdot (W1 \cdot X_2 + W2 \cdot X_2)$, where F^e - appropriate function of mixture (excess volume or excess energy etc.); X_1 and X_2 - mole fractions of components of a binary solid solution 1-2; and W1 and W2 - constant of the equation of Margules (Saxena, 1975, [4]). The designed Margules parameters for the description of excess volume of (Ca, Sr)-zirconium- phosphate are equal: W1 = -2.25 (55); W2 = 3.67 (41) cm^3/mol.

$V^e = X \cdot (1-X) \cdot [-2.25 \cdot X + 3.67 \cdot (1-X)]$ (5)

The equation (5) describes excess volume of mixture with an accuracy of 0.2 cm^3/mol.

References:

1. Volkov Ju.F., Orlova A.I. Formula types systematics of orthophosphates of one -, two -, three-, four- and five- valency elements. Radiochemistry, 1996, v.38, ¹ 1, pp.15-21.

2. Burnham C.W. // Least-squares refinement of crystallographic lattice parametres for IBM PC/XT/AT and compatibles, Harward University, Cambridge MA02138, 1991 (program description), 24p.

3. Chichagov A.V. // Information-calculating system on crystal structure data of minerals (MINCRYST). Materials Science Forum, volks 166-169, 1994, p. 187-192. Trans. Tech. Publications, Switzerland, 1994.

4. Saxena S. Thermodynamics of solid solutions of rock forming minerals. M., World, 1975, 205pp.

#**Suvorova V.A., Kotelnikov A.R., Ushakovskaya T.V., Tikhomirova V.I. Properties of synthetic zirconates (zirconalites, zirconium-perovskites)**

key words: [*circonates, synthesis, chemical and physical properties, parameters of the elementary cell*]

The main problem of this investigation is the study of chemical and physical properties and definition of the parameters of the elementary cell (PEC) of synthesized accesory minerals (circonate type). Mainly, these minerals are solid solutions and potential matrices for the fixation of alkaline, alkaline- and rare-earth elements (Cs, Sr, Ba, Ce, Eu etc) which can enter the crystalline lattice of minerals as isomorphous impurities replacing the atoms Ca, Ba and partially Zr. A high stability for a physico-chemical effect makes it possible to consider this material as perspective for the use as a matrix to displace RAW-elements.

Mineral synthesis is performed by a hot pressing method in 3 stages: 1) drying of the charge in vacuum during 0.5 hour; 2) pressing at 1350^{0}C and axis pressure of 300 bar during 0.5 hour; 3) completing synthesis at 1350^{0}C and remaining axis pressure (50 bar) during 4 hours [1]. Synthesized solid solution of zirconates represent the samples of poly- and monomineral ceramics with the density of 88-98% of the theoretical one. Chemical composition, equations of synthesized matrices and stable phases of the stadied part of the system CaO - (SrO) - (EuO) - TiO - CeO$_2$ are given in Tabl.1 (according to microprobe data).

For some of these synthesized zirconates the parameters of the elementary cell (PEC) are calculated. The results of the calculations are given in Tabl.2 (the errors of some more exact definitions are given in brackets and refer to the last decimal signs).

Table1. Contens of oxides (wt%) and formulas of samples

N sample	Mineral phase	CaO	SrO	TiO$_2$	ZrO$_2$	Formula
1101/1	Zrnlt[a]	47.00	-	50.53	2.47	$Ca_{1.1}(Ti_{0.81}Zr_{0.20})_{2.9}O_{6.9}$
	Prv[b]		-	59.58	13.12	$Ca_{1.9}(Ti_{0.94}Zr_{0.06})_{2.1}O_{6.1}$
1102/1	SrZrnlt[c]	18.47	8.067	54.27	19.20	$(Ca_{0.7}Sr_{0.3})_{1.1}(Ti_{0.7}Zr_{0.3})_{2.9}O_{6.9}$
	SrPrv[d]	7.976	14.81	87.42	2.05	$(Ca_{0.7}Sr_{0.3})_2(Ti_{0.94}Zr_{0.06})_{2.1}O_{6.1}$
1106/1	Zr-Prv[e]	41.21	-	-	58.79	$Ca_{1.98}Zr_{2.02}O_{6.02}$
	Tzr[f]	21.95	-	-	78.05	$Ca_{0.9}Zr_{3.1}O_{7.1}$
1103/1			Eu$_2$O$_3$			
	EuZrnlt[g]	26.36	1.991	50.16	20.99	$(Ca_{0.93}Eu_{0.07})_{1.2}(Ti_{0.7}Zr_{0.3})_{2.9}O_{6.9}$
	EuPrv[h]	48.16	1.564	49.29	0.72	$(Ca_{0.96}Eu_{0.04})_2(Ti_{0.99}Zr_{0.01})_2O_{6.0}$
1126/1	EuZr-Prv[i]	36.88	11.05	-	52.25	$(Ca_{0.74}Eu_{0.26})_{1.99}Zr_{2.01}O_{6.01}$
	EuTzr[j]	37.38	10.55	-	51.75	$(Ca_{0.8}Eu_{0.2})_{0.91}Zr_{3.09}O_{7.09}$
Ст 17/2	SrZr-Prv[k]	SrO 43.44	0.522	-	56.01	$(Sr_{1.89}Eu_{0.018})_{1.908}Zr_{2.04}O_{6.0}$
1130/1	EuCrt[l]	6.676	3.630	41.55	48.14	$(Ca_{0.6}Eu_{0.4})_{1.2}(Ti_{0.43}Zr_{0.57})_{2.57}O_{7.57}$
	EuZr-Prv	22.36	0.462	-	76.18	$(Ca_{0.56}Eu_{0.04})_{1.98}Zr_{2.02}O_{6.02}$

Table 2. Parameters of the elementary cell of some zirconates.

N sample	Basic phase	a, E	b, E	c, E	α, °	β, °	γ, °	V, (E)³
1101/1	Zrnlt mono*[2]	12.436 (2)	7.220 (1)	11.480 (1)	90.00	100.27 (1)	90.00	1014.3 (2)
1102/1	SrZrnlt mono*[2]	12.428 (8)	7.224 (4)	11.480 (6)	90.00	100.07 (6)	90.00	1015.4 (9)
1103/1	EuZrnlt mono*[2]	12.443 (3)	7.228 (3)	11.476 (4)	90.00	100.31 (3)	90.00	1015.4 (5)
1106/1	Zr-Prv orto*[3]	5.757 (2)	8.012 (2)	5.592 (1)	90.00	90.00	90.00	257.9 (09)
1126/1	EuZr-Prv orto*[3]	5.742 (8)	7.921 (9)	5.924 (8)	90.00	90.00	90.00	269.5 (5)
Ст 17/2	SrZr-Prv orto*[3]	5.807 (1)	8.195 (2)	5.804 (1)	90.03 (1)	90.46 (1)	89.76 (1)	276.24 (6)
1130/1	EuCrt mono*[2]	12.445 (7)	7.225 (2)	11.483 (3)	90.00	100.32 (2)	90.00	1015.8 (7)

Note: * - structure in the approximation of which the calculation was made. These samples of zirconates were tested on leaching of Sr, Ca and Zr.

Table 3. Velocities V(g/m²/day) of Sr leaching from the ceramic matrix of the NZP (sodium zirconium phosphates) type and synthetic zirconates.

Mineral phase	Density, g/sm³	Wt% Sr of initial sample	0-1 days	1-7 days	7-14 days	7-28 days	References
NZP+Mz*+ZP** +CsZP***	3.23	0.47	-	0.007	-	0.030	[6]
(Ca,Sr)ZrO₃ - SrZr-Prv	4.18	9.28	9.13	1.080	0.304	-	This work N 1125/1
(Ca,Sr)Zr₃O₇ - SrTzr	4.99	5.40	3.76	0.556	0.171	0.095	This work N 1128/1
(Ca,Sr)Zr₂TiO₇ - SrZrnlt	5.04	8.72	4.36	0.440	0.097	0.039	This work N 1131/1
SrZrO₃ - SrZr-Prv	4.90	36.74	42.9	2.300	-	0.630	This work N Ст17/2

Note: * - monazite; ** - ZrP_2O_7; *** - Cs-bearing ZrP_2O_7.

Table 4. Velocities V(g/m²/day) of Ca leaching from the natural minerals, ceramic matrix of the Synroc type and synthetic zirconates.

Mineral phase	Density, g/sm³	Wt% Ca of initial sample	0-1 days	1-7 days	7-14 days	7-28 days	References
Pl*	2.76	7.750	0.63	0.090	0.043	0.013	[4]
Synroc-C	~4.5	6.700	-	0.003	-	0.006	[5]
CaZr₂TiO₇ - Zrnlt	4.28	10.47	0.30	0.025	0.009	0.021	This work N 1122/1
(Ca,Sr)ZrO₃ - Zr-Prv	4.18	16.19	2.14	0.075	0.131	-	This work N 1125/1
(Ca,Sr)Zr₃O₇ - SrTzr**	4.99	5.401	1.43	0.179	0.065	0.054	This work N 1128/1
(Ca,Sr)Zr₂TiO₇ - SrZrnlt	5.04	6.020	0.54	0.051	0.025	0.012	This work N 1131/1
(Ca,Eu)ZrO₃ EuZr-Prv	4.58	15.88	1.77	0.190	-	0.037	This work N 1126/1
SrZrO₃ - SrZr-Prv	4.90	0.151	57.6	5.170	-	0.840	This work N Ст17/2
(Ca,Eu)ZrTi₂O₇ - EuCrt	4.84	6.262	1.23	0.049	-	0.013	This work N 1130/1

Note: * - natural plagioclase; ** - Sr-bearing tazheranite.

Table 5. Velocities V(g/m^2/day) of Zr leaching from the ceramic matrix of the Synroc type, of the NZP type and synthetic zirconates.

Mineral phase	Density, g/sm^3	Wt% Zr of initial sample	0-1 days	1-7 days	7-28 days	References
Synroc-C	~4.5	5.6		1×10^{-6}	10×10^{-7}	[5]
NZP+Mz+ZP +CsZP	3.23	22.8		4×10^{-6}	3.1×10^{-7}	[6]
SrZrO$_3$ - SrZr-Prv	4.90	41.47	1.2×10^{-4}	3.1×10^{-3}	5.1×10^{-4}	This work N St17/2
(Ca,Eu)ZrO$_3$ - EuZr-Prv	4.58	45.2		1.2×10^{-4}	6.7×10^{-6}	This work N 1126/1
(Ca,Eu)ZrTi$_2$O$_7$ - EuCrt	4.84	23.68				This work N 1130/1

Table 6. Velocities V(g/m^2/day) of Eu leaching from synthetic zirconates.

Mineral phase	Density g/sm^3	Wt% Eu of init. sample	0-1 days	1-7 days	7-28 days	References
(Ca,Eu)ZrO$_3$ - EuZr-Prv	4.58	15.0	2.8×10^{-4}	2.1×10^{-4}	5.0×10^{-4}	This work N 1126/1
(Ca,Eu)ZrTi$_2$O$_7$ - EuCrt	4.84	15.84	1.2×10^{-4}	5.5×10^{-5}	1.6×10^{-5}	This work N 1130/1

Low velocities of leaching Ca, Sr and Zr showed quite high stability of solid solutions of zirconates, constituting synthesized samples, comparable with the stability of Sinrok-C [5], natural monocrystals of plagioclase [4] and ceramic matrix of the NZP type [6]. It testifies to a possibility to use these solid solutions of zirconates as matrix materials - fixators of alkaline, alkaline-earth radionuclides of RAW (radioactive waste). Rather high velocities of leaching from the sample N St17/2 can be probably explained by the fact that it was made not by the hot pressing method, but by sample annealing at 1240^{0}C, so the initial components can be present in the sample.

Moreover, the samples of zirconates were tested on Eu-leaching from them. The results given in Tabl.6 testify to the zirconate applicability as matrices, keeping europium.

References:

1. Martynov K.V. et al. Synthesis and study of the composition and properties of ceramic matrices on the basis of minerals of complex oxide group bearing elements-imitators of RAW // 4th Annual Scientific & Technical Conference of the Nuclear Society «Nuclear Energy and Man Security NE-93» June 28- Jule 2, 1993, Nizhni Novgorod, Abs. of Conf, part.II, pp.968 - 969 (in Russian).
2. PDF, N 34-167.
3. PDF, N 35-790
4. Kotelnikov A.R., Akhmedzhanova G.M. and Suvorova V.A. Minerals and their solid solutions - matrices for immobilization of radioactive waste // Geochemistry, 1999, N 2, pp.1-9, (in Russian).
5. Ringwood A.E et al. SYNROC. In: Radioactive waste forms for the future (eds. Lutze and Ewing).1988, ch.4, pp.232-334.

[#]Bondar' A.M.[1], Kozerenko S.V.[2], Rebrov A.I.[2] Proton magnetic resonance in synthetic zinc sulfides

[1] Baikov Institute of Metallurgy and Material Science, Russian Academy of Science
[2] Vernadsky Institute of Geochemistry and Analytical Chemistry, Russian Academy of Science

key words [*proton magnetic resonance, zinc sulfides, synthesis, properties*]

Sulfide compounds which comprise a number of mineral species are known to have a numerous set of useful properties: from valuable electrophysical, optical, semiconductive (thermoelectric driving forces, photo - and X-ray luminescent etc.) up to important for mineralogy and geochemistry typomorphic criteria used in prospecting and estimates of rare metal ore deposits. The traditional X-ray diffraction and crystallochemical studies cannot give a direct answer to the question: why sulfides are characterized by such variable physical, chemical and electrophysical properties? We used direct radiospectrometric methods such as nuclear magnetic resonance (NMR) and specifically the proton magnetic resonance (PMR) of broad bands. This allowed to prove the existence of hydrogen-bearing groups in the crystalline structure of minerals in question and in their artificial analogs. Besides, the possibility of heterovalent isomorphous substitution in their anion sublattice was demonstrated. It means that S^{-2} atoms could be partly substituted for hydroxyl and (or) hydrosulfide groups, so that the possibility of compositional and property variations of these compounds are markedly enlarged (Bokij, Bondar', 1978; Kalinichenko et al., 1981; Kozerenko et al., 1995) [1-3].

It should be pointed out that the differential discrimination of proton-bearing groups forming different chemical bond types in sulfides was attained only by use of spe-

cial high resolution PMR technique. This method allows the averaging of strong dipole-dipole interaction and separation of different types of chemically nonequivalent protons in the composition of the studied samples.

High-resolution PMR spectra of synthetic sphalerites (ZnS) obtained at different temperatures in the process of hydrothermal synthesis were recorded. Several types of hydrogen-bearing groups were revealed. PMR spectra were registered at room temperature on Bruker MSL-300 Spectrometer at a frequency of 300,130 MHz by use of special CRAMPS (Combination Rotation And Multiple Pulse Sequence) techniques. This techniques allowed to use MREV-8 pulse sequence for elimination of 'H homonuclear dipole-dipole interaction along with sample rotation at magic angle (54,4°) in order to average the chemical shift tensor anisotropy as well as to average more weak heteronuclear magnetic dipole-dipole interaction. Sample rotation velocity was 2.5-3 kHz, 90° pulse duration was 1.5 μs, δ-chemical shifts in PMR spectra were measured in relation to tetramethylsilane.

Up to five different types of chemically nonequivalent proton-bearing groups are distinctly revealed on PMR spectra, the former being determined both as hydroxyl and hydrosulfide groups. The comparison of PMR data on synthetic ZnS obtained for low synthesis temperature (25°C) showed that the protons probably are related to oxygen atoms in hydroxyl groups and/or water of hydration and having the chemical shift within δ=4.3-4.8 ppm and comprise the significant fraction of total proton content. PMR spectra of ZnS obtained as a result of higher synthesis temperature (50, 100, 150, 200, 250°C) are characterized by the total proton content increase along with decreasing synthesis temperature mainly at the expense of broad component within the range of δ=4.3-0.27 ppm the signal components with chemical shifts of different chemically nonequivalent protons belonging to oxygen-and sulfur-bearing groups are distinctly observed. With synthesis temperature increase from 25°C up to 150°C (see fig.1) the abrupt decrease of broad component of δ~ 4.3 ppm line is accompanied by the increase of narrow component (δ= 3.1, 1.74, 0.75, 0.27 ppm) line relative to intensity which is probably caused by isolated and located protons.

Thus the variation of chemical shift and spectra component broadness along with the synthesis temperature increase is considered as the indication of the existence of chemically nonequivalent hydrogen atoms (up to five types of those) taking part in different hydrogen bonds at the expense of heterovalent isomorphism in the anion sublattice. The proton existence in the crystalline lattice of sulfides evidently has a substantial influence on the electrophysical (semiconductive) and optical (luminescent) properties of synthetic zinc sulfides.
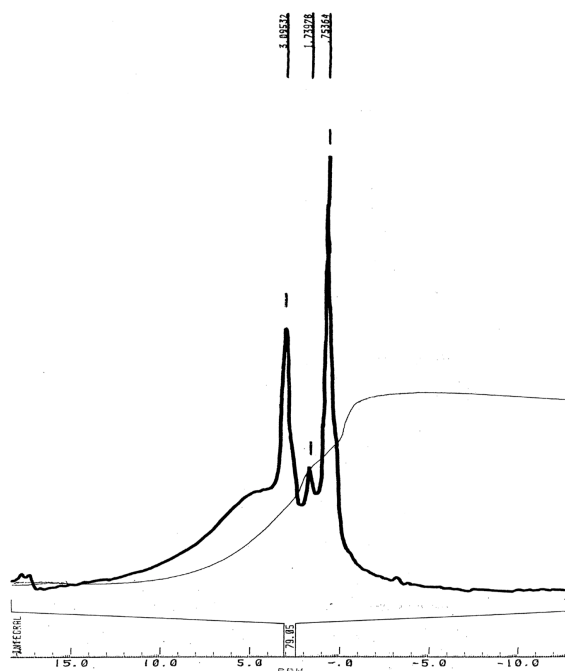
Fig.1. The high-resolution solid-state proton magnetic resonance spectrum recorded at room temperature on Bruker MSL-300 Spectrometer on a frequency of 300,130 MHz by use CRAMPS techniques from the powdered sample of zinc sulfide synthesized at 150°C.

References:

1. Bokij G.B., Bondar' A.M. On the role of hydrogen in sulfide crystal structure// Dokl. AN SSSR.1979. Vol.248. N4. P.956.
2. Kalinichenko A.M., Matjash I.V., Galiy S.A. et al. Proton magnetic resonance in pyrites of different origin // Geokhimiya. 1982. N5. P.765.
3. Kozerenko S.V., Khramov D.A., Fadeev V.V. et al. A study of pyrite formation mechanism in aqueous solutions at low temperatures and pressures // Geokhimiya. 1995. N9. P.1352.

Ogorodova L.P.[1], Melchakova L.V.[1], Kiseleva I.A.[1], Peretyazhko I.S.[2], Zagorsky V.E.[2] Thermodynamic properties of lithium tourmaline – elbaite

M.V.Lomonosov Moscow State University, Geological department, Vorobjevy Gory Moscow 119899
[2] Institute of Geochemistry, Academy of Sciences, Favorsky str., 1a, Irkutsk, 664033, Russia mineral@geol.msu.ru

key words: [*tourmaline, elbaite, liddicoatite, calorimetry, heat capacity, entropy, enthalpy and Gibbs free energy of formation*]

The thermodynamic modelling of boron mineralization in different natural processes needs the reliable thermochemical data on tourmalines. The previous experimental determination of thermodynamic properties has been made only for alumodravite [1]. The study of thermodynamic parameters of tourmalines of other composition was initiated by us with thermochemical investigation of natural lithium tourmaline – liddicoatite-elbaite.

We chose for investigation a sample of natural elbaite from pegmatites East Siberia [2]. Its chemical composition and structural characteristics were determined. The tourmaline studied has high contents of Li_2O (2.34 %) and CaO (2.65 %) and can be considered as calcium elbaite - liddicoatite. The formula of tourmaline investigated was calculated for 31 anions: $(Na_{0.49}Ca_{0.45}K_{0.02})_{0.96}(Li_{1.49}Mn_{0.05}Fe^{+3}_{0.03}Mg_{0.09}Al_{7.20})_{8.86}Si_{6.16}B_{3.13}O_{27.91}(OH)_{2.64}F_{0.45}$.

The thermochemical investigations were performed in differential scanning calorimeter DSC «Mettler TA-2000B» and high-temperature heat-flux Calvet microcalorimeter «Setaram».

The heat capacity of lithium tourmaline was measured by DSC method in the interval of 110 – 800 K in flowing nitrogen with a heating rate of 10 K/min and a cooling rate of 5 K/min. Details of instrument operation are described in [3]. The molar enthalpy and melting temperature of indium reference substance (99.9999 % purity) were used to calibrate the DSC.

The values of enthalpy increments $H^o_T-H^o_{298.15}$ of the mineral studied were measured in Calvet microcalorimeter by the «drop» method at the temperatures T=712, 803, 973 K. The calibration of the calorimeter was achieved by dropping pieces of corundum α-Al_2O_3. The DSC measurements results in the interval of 290-650 K and Calvet microcalorimeter experimental data were fitted by least-squares yielding with respective average deviation of approximation presented in brackets:

$C°p = 982.88 + 313.69 \cdot 10^{-3}T - 274.70 \cdot 10^5 T^{-2}$ J/mol·K

($\pm$ 1,3%) at 298.15-800 K,

$C°p(298,15) = 767.4$ J/mol·K;

$H^o_T - H^o_{298.15} = 982.88 T + 156.84 \cdot 10^{-3}T^2 + 274.70 \cdot 10^5 T^{-1} - 399119.24$ J/mol.

The enthalpy of formation of liddicoatite-elbaite was determined in Calvet microcalorimeter by high-temperature melt solution calorimetry. The dissolution in solvent $2PbO \cdot B_2O_3$ at T=973 K was made using the specialty designed equipment which was described in [4]. To calibrate calorimeter the «drop» method of Pt wire was used. A precision of weighing the samples was $\pm$ $2 \cdot 10^{-3}$ mg.

The enthalpy of formation of liddicoatite-elbaite from the elements was calculated from experimental values of heat of the solution of mineral studied and constituent oxides and fluorides, the experimental and reference data on enthalpy increments $H°_{973}$- $H°_{298.15}$ and enthalpies of formation $\Delta H^o_f(298.15)$ of oxides and fluorides.

The standard entropy at T=298.15 K was estimated from the exchange reaction between elbaite and alumodravite investigated in [1] by the low-temperature adiabatic calorimetry method.

On the basis of the obtained in this work values of $\Delta H^o_f(298.15)$ and $S^o(298.15)$ the free Gibbs energy of formation from the elements $\Delta G^o_f(298.15)$ of liddicoatite-elbaite

$(Na_{0.49}Ca_{0.45}K_{0.02})_{0.96}(Li_{1.49}Mn_{0.05}Fe^{+3}_{0.03}Mg_{0.09}Al_{7.20})_{8.86}Si_{6.16}B_{3.13}O_{27.91}(OH)_{2.64}F_{0.45}$

was calculated.

Table. Thermodynamic properties of natural liddicoatite-elbaite $(Na_{0.49}Ca_{0.45}K_{0.02})_{0.96}(Li_{1.49}Mn_{0.05}Fe^{+3}_{0.03}Mg_{0.09}Al_{7.20})_{8.86}$ $Si_{6.16}B_{3.13}O_{27.91}(OH)_{2.64}F_{0.45}$ at T=298.15 K (M.м.=948.13g/mol)

$C^o p$, J/mol·K	S^o, J/mol·K	ΔH^o_f, kJ/mol	ΔG^o_f, kJ/mol
767.4	624.1*	-15555.7±2.1	-14613.5

*-estimated from the exchange reaction

References:

1. Kuyunko N.S., Semenov Yu.V., Gurevich V.M., Kuzmin V.I., Topor N.D., Gorbunov V.E. Experimental determination of thermodynamic properties of tourmaline - dravite. Geokhimiya, 1984, N 10, p.1458-1465.
2. Zagorsky V.E., Peretyazhko I.S. Pegmatites with gemstones of Central Zabaikalja. Novosibirsk: Nauka, 1992, 224 p.
3. Topor N.D. & Melchakova L.V. Measurement of heat capacity of minerals in scanning regime by quantitative differential thermal analysis. Vestn.Mosk.Univ., 1982, N 6, p.50-58.
4. Topor N.D., Kiseleva I.A., Melchakova L.V. The equipment for determination of the heats of solution of inorganic compounds and minerals by high-temperature microcalorimetry method. Zh.Phys.Chem., 1980, N 2, p.521-523.

#Melchakova L.V.[1], Ogorodova L.P.[1], Kiseleva I.A.[1], Belitsky I.A.[2] Investigation of natural phillpsite group zeolites by thermal analysis method and differential scanning calorimetry

[1] M.V.Lomonosov Moscow State University, Geological Department, Vorobjevy Gory, Moscow, 119899, mineral@geol.msu.ru
[2] Institute of Mineralogy and Petrography, Academy of Sciences, Novosibirsk, 630090

key words: [*zeolite, harmotome, phillipsite, thermal and thermogravimetric analyses differential scanning calorimetry, heat capacity, dehydration*]

Phillipsite and harmotome form a continuous series of solid solution with common formula $(K,Na,Ca_{0.5},Ba_{0.5})_x[Al_xSi_{16-x}O_{32}] \cdot 12H_2O$, where x≅4-7 [1]. K, Na, Ca may be the most abundant extra-framework cation, but the name harmotome is retained for the Ba-dominant member of the series.

The dehydration of zeolites processes are important in a variety of applications including pollution abatement, catalysis and gas separation. The thermal stability is connected with the ratio of Si/Al, content of exchanged cations and framework topology.

We studied the samples of natural phillipsite (Khibiny, Russia) and harmotome (Rodopy, Bulgaria). The samples have been examined by X-ray and electron microprobe analyses. The formulae calculated for 32 oxygens were the

following: phillipsite $(K_{3.05}Na_{0.53}Ca_{1.26}Sr_{0.04}Ba_{0.03})$ $[Al_{5.57}Si_{10.26}O_{32}]\cdot11.67H_2O$ and harmotome $(Ba_{2.03}Na_{0.06}K_{0.07}Ca_{0.12}Sr_{0.02})[Al_{5.13}Si_{11.02}O_{32}]\cdot12.05H_2O$.

The Si/Al ratio in phillipsite (1.84) and harmotome (2.15) shows that they are zeolites with median silicon content. The water content was determined by weighing the samples before and after heating at T=700°C with an error $\pm2\cdot10^{-6}$g.

The zeolites thermal behavior was studied by differential thermal (DTA) and thermogravimetric (TG and DTG) analyses in temperature interval of 20-1300°C with heating rate of 15°/C by using derivatograph «Q-1500 D». Harmotome and phillipsite are nonstable at heating and begin to loss water at room temperatures. Harmotome, with five different water sites in the structure, looses its water in four steps: I – in the interval of 40-80°C, II – 80-230°C (T_{max} = 200°C), III – 230-310°C (T_{max} = 290°C), IV – 310-440°C (T_{max} = 320°C). The total water loss was equal to 14.8%.The harmotome structure is destroyed near 440°C and the new phase is formed at T=720°C, this process is accompanied by exothermal effect. Phillipsite looses its water in five steps: I – in the interval of 50-100°C, II – 100-180°C, III - 180-270°C (T_{max} =205°C), IV – 270-330°C, V – 330-500°C (T_{max} = 380°C). All water (15.6%) is eliminated at temperature 500°C. Our experiments showed that the new stable phases form at heating above 700°C and the following rehydration doesn't take place. It may be connected with significant constraction of the zeolite structure.

The thermochemical study of the natural phillipsite of the composition $(Na_{1.08}K_{0.80})[Al_{1.88}Si_{6.12}O_{16}]\cdot6H_2O$ was performed early by adiabatic calorimetry method in the interval of 15-300 K, the value of standard entropy at T=298.15 K was calculated [2]. There are no publications on thermodynamic properties of harmotome.

The thermodynamic characteristics were investigated by differential scanning calorimery method (DSC «Mettler TA-2000 B»). Details of instrument operation are described in [3].

The enthalpies of total dehydration of zeolites studied were measured by the DSC method. The values obtained were the following: $\Delta H^o_{dehydr.}$ = 1116 kJ/mol for harmotome in the temperature interval of 40-440°C and 991 kJ/mol for phillipsite in the interval of 50-500°C. The average bonding strengths of water with zeolite structure relatively to steam H_2O are 93 kJ (harmatome) and 85 kJ (phillipsite) per one mole of water.

The low-temperature heat capacities of natural zeolites were measured by DSC method in the interval of 110 – 320 K in flowing nitrogen with a scanning rate of 5-10 K/min. The molar enthalpy and melting temperature of indium reference substance (99.9999 % purity) were used to calibrate the DSC. The standard heat capacities of phillipsite-K $C^o p(298.15)$=1645.2 J/mol·K and harmotome $C^o p(298.15)$=1602.0 J/mol·K were obtained. The specific heat capacities of phillipsite-K studied in this work (1.218 J/g·K) and phillipsite-Na investigated by adiabatic calorimetry in [2] (1.223 J/g·K) are in a agreement within experimental errors (1-1.5%). The molar values differ because of their composition differences ($C^o p(298.15)$=1572.4 J/mol·K for phillipsite-Na [2]). It was the first thermochemical investigation of harmotome.

References:

1. Coombs D.S. et al. Recommended nomenclature for zeolite minerals: Report of the subcommittee on zeolites of the International Mineralogical Assotiation, Commission on New Minerals and Mineral Names. Eur.J.Mineral., 1998, 10, p.1037-1081.
2. Hemingway B.S. & Robie R.A.. Thermodynamic properties of zeolites: low-temperature heat capacities and thermodynamic functions for phillipsite and clinoptilolite. Estimates of the thermochemical properties of zeolitic water at low temperature. Am.Miner., 1984, v.69, p.692-700.
3. Topor N.D., Melchakova L.V.. Measurement of heat capacity of minerals in scanning regime by quantitative differential thermal analysis. Vestn.Mosk.Univ., 1982, N 6, p.50-58.

#Khokhryakov A.F. Experimental study of the formation of rounded diamond crystals

Institute of Mineralogy and Petrography SB RAS pr. Koptyuga, 3, Novosibirsk 90, 630090

key words: [*diamond dissolution forms, morphology, experiment*]

At present, most of the scientists do not question the formation of rounded natural diamonds of octahedroid, dodecahedroid and tetrahexahedroid type in the process of post-growth evolution of the flat-faced crystals. Yet, the problem of the nature of such process and the composition of the medium, influencing diamond, remains open to discussion. This leads to the appearance of a new term, "resorption", for describing a non-specific process which has, subsequent to diamond growth diminished the size of the diamond, whether it be by oxidation, graphitization or some other mechanism [1]. In previous works [2-4] we had shown that in the process of dissolution in aqueous silicate melts, the dissolution forms, morphologically similar to the natural semi-rounded diamond crystals, developed. However, in such experiments synthetic diamond crystals were used, and dissolution was followed only up to 15-20% loss of their initial mass. In the present work, the experimental results of deep dissolution of the main habit types of natural diamond in the model carbonate and silicate systems are presented.

The experiments were held on the high-pressure apparatus of the "split-sphere" type at the pressure 5.0-5.5 GPa in the temperature range 1350-1450°C, in accordance with the previously published technique [5]. In the experiments, the carbonates Na_2CO_3, $CaCO_3$, $MgCO_3$ and silicate $CaMgSi_2O_6$ were used. The purity of the reagents was not less than 99,9 wt %. Carbonate or silicate powder (120-130 mg), distilled water (20 wt %) and diamond crystals were put into platinum ampoules, which then were hermetized by arch-welding. For the purpose of dissolution, natural octahedrons, pseudo-dodecahedrons and cubes 0,5-1,0 mm in size from the "Udachnaya" and "Ajkhal" kimberlite pipes, along with cubooctahedral synthetic dia-

mond crystals, were used. In each experiment the number of crystals was 10, with their bulk mass of 3,5 up to 5,5 mg. Dissolution of the crystals was stated according to the changes of their weight, decrease of their geometrical size and changes of macro- and micromorphology. In the experimental series with their duration from 1 to 40 hrs, the evolution of crystals' forms, up to their complete dissolution, was followed. There were not found any essential morphological differences for the forms of diamond dissolution in the carbonate or water-silicate systems. Dissolution of the crystals in all the studied systems proceeded according to one scheme.

At the initial stage of diamond dissolution the negatively oriented trigons and ditrigonal layers of dissolution form on the {111} faces, while on the {100} faces, tetragonal pits occur. At crystal edges, the rounded surfaces with the sheaf-like or hackle striation, drop-like hills and facial juncture, develop. In the course of dissolution, the rounded surfaces expand and, finally, totally destroy the initial crystal faces. The initial faces of octahedral crystals disappear completely after dissolution of more than 20 wt %, at the same time, the crystal still maintains its octahedral habit and can be characterized as octahedroid. The initial faces of natural cubes disappear after dissolution of more than 50 wt %, and the crystal attains the characteristic form of tetrahexahedroid. Dissolution of pseudo-dodecahedrons manifests itself in gradual rounding of the {110} pseudo-faces. On crystals of all the types, ditrigonal layers around the [111] apexes and facial junctures are present. In the process of further dissolution, the crystals become more and more rounded and lose their initial shape completely, taking the spherical form, typical for the so-called natural diamonds of the Ural type.

Thus, the obtained results represent the first experimental proof of the formation of dodecahedroids, octahedroids and tetrahexahedroids of natural diamond in the process of dissolution of the flat-faced crystals. Considering the previously obtained results on diamond dissolution in anhydrous silicate [2] and carbonate [6] melts, the conclusion can be made, that it is the presence of water in the reaction medium that has the particular importance for the formation of natural diamond rounded crystals. Kimberlite and lamproite magmas, transporting diamond from the upper mantle, are the most probable water-containing carbonate-silicate media reactional relative to natural diamond.

References:

1. Otter M.L., Gurney J.J. Mineral inclusions in diamonds from the Sloan diatremes, Colorado-Wyoming State Line kimberlite district, North America// Kimberlites and Related Rocks (ed. J. Ross), Geological Society of Australia, Spec. Publ. 1986.N 14. V.2. Blackwell, Oxford. P.1042-1053.
2. Chepurov A.I., Pal'yanov Yu.N., Khokhriakov A.F., Sonin V.M., Sobolev N.V.. On the forms of dissolution of diamond crystals in the silicate melts at high pressure// Dokl.AN SSSR. 1985. V.285. №1.P.212-216.
3. Khokhriakov A.F., Pal'yanov Yu.N. Morphology of diamond crystals, dissolved in the aqueous silicate melts // Mineral. Zhurnal. 1990. V.12. №1. P.14-23.
4. Pal`yanov Yu.N., Khokhriakov A.F., Borzdov Yu.M., Sokol A.G. On the Role of Water in Growth and Dissolutions of Diamond // Proceeding of 8 Int. Symp. on Water-Rock Interaction (WRI-8) Vladivostok, Russia , 1995, Balkema, Roterdam. Eds I.Haraka and O.Chudaev. P.95-98.
5. Pal'yanov Yu.N., Khokhriakov A.F., Borzdov Yu.M., Sokol A.G, Gusev V.A., Rylov G.M., Sobolev N.V.. Growth conditions and real structure of synthetic diamond crystals// Russian Geology and Geophysics. 1997. V.38. №5. P.920-945.
6. Khokhriakov A.F., Bajev D.A., Pal'yanov Yu.N. Forms of growth and dissolution of diamond crystals in CaCO$_3$-C system // IV International conf. "Crystals: growth, real structure, application" Alexandrov. 1999. V.1. P.337-341.

Sonin V. M. Etching of diamonds in silicate melts in contact with atmospheric medium

Institute of Mineralogy and Petrography SB RAS ac. Koptjug ave., 3, Novosibirsk, 90, 630090 chepurov@crystal.nsib.ru turkin@uiggm.nsc.ru

The formation of diamonds, connected genetically with the mantle peridotites and eclogites, occurred at the high P-T parameters, corresponding to the fields of their thermodynamic stability. Most authors agree, that the evacuation of diamonds to the surface had to happen quickly enough, in order to provide their safety in the fluid-saturated kimberlitic magma. Diamond interaction with silicate melts, for a first approach, can be modelled at the atmospheric pressure, though, naturally, the diamond-containing kimberlite magma existed at higher pressures.

Within the frames of the work, we have studied the etching peculiarities of diamond crystals in the fusible silicate melts: Na$_2$O (30 wt. %) - SiO$_2$ (70) (No 1), Na$_2$O (20) - B$_2$O$_3$ (40) - SiO$_2$ (40) (No 2), as well as in natural alkaline basalt. The necessity of such study was caused by the fragmentary character of such investigations and, correspondingly, rather contradictory data on the subject. The experiments were held at the device, constructed on the base of a tubular electric heater of the SUOL type, in platinum ampoules at 1000-1200°C in the atmospheric medium. Yet, only the experiments, in which diamond was not in the direct contact with the air, were taken into account. For etching, the powdered natural crystals of the fraction 0,6/0,8 mm, and single natural diamond crystals of octahedral habit, weighing 4,4-15,1 mg, were used. The portion of diamond "powder" amounted to 7±0,2 mg (35±1 grains) per one experiment.

The provided investigation allowed to establish, that (1) at 1000°C the silicate melt reduces the rate of diamond etching, relative to the atmospheric air (some 2,5-1,5 orders in the row of compositions No1, No2 and the mixture of No2 and basalt (1:1 by weight); (2) in the silicate melt, contacting with the air, diamonds are oxidated by the dissolved oxygen; (3) the rate of the process and the morphology of the etched crystals probably depend on the transport characteristics of a melt.

During the microscopic study of the samples it was established, that in the process of such etching of diamonds in silicate melt, the gaseous bubbles, i.e. the products of diamond oxidation, generate on the crystal surfaces. The morphological changes were studied in the experiments with single crystals. In the melt No1, the irregularly developed dull spots occurred on the faces, along with the blackening of the surfaces. The elements of such dull spots - crystallografically disoriented geometrically irregular etch pits - serve as indicators of the corrosion sculptures, occurring during the surface graphitization of diamonds. The presence of non-diamond carbon on the crystals was confirmed by the IR-spectroscopy of the samples. At some parts of the faces, the minute (up to first mkm in size) reversely oriented triangular etch pits were found, as a rule, with distorted outlines. In the melt No2, against the growth of etching rate, numerous disc sculptures 20-260 mkm in size, consisting of minute irregular etch pits, were found on crystal surface. Such disc sculptures represent the imprints of gas bubbles - the products of oxidation. In the course of diamond crystal etching in the melt, consisting of synthetic composition No2 and basalt mixture (1:1 by weigh), the triangular pits, oriented in accordance with to the face outlines, were formed. All the etch figures are known for natural diamonds.

In the experiments with basalt melt, conducted at 1130-1200°C, it was established that: (1) due to the high rate of diamond oxidation and low solubility of the gaseous products of the reaction between the diamonds and the etching melt, the "foam-like" layer of bubbles forms, rising the crystals to the surface, so that diamond etching occurs in the surface layer of the melt; (2) in contrast to the oxidation in gaseous medium, diamond etching in the basalt melt proceeds selectively, with the formation of flat-bottomed steep-walled triangular, with truncated apexes, and hexahedral pits, along with the caverns with more complicated outlines. As a result of the etching, diamond grains are deeply corroded and obtain irregular forms, with greater specific surface. The character of etching of singular monocrystals is essentially similar: selective etching with the formation of deep caverns, usually flat-bottomed, with one or a number of smaller gently sloping triangular etch pits, directly oriented relative to the faces. The etch figures, obtained in the basalt melt, are morphologically similar to the faceted caverns on the natural diamonds from lamproites, while the surface, consisting of numerous caverns of various sizes, reminds the so-called cell-comb sculptures on the impact diamonds.

So, under practically similar outer conditions, varying only chemical composition of the melt, we obtained a very wide spectrum of morphological peculiarities, previously fixed only in sharply oxidizing (directly oriented triangular etch pits), or reducing conditions (corrosion sculptures due to surface graphitization). The most wide-spread type of partially dissolved natural diamonds is characterized by the presence of reversely oriented triangular etch pits on the {111} faces, which form under the conditions of intermediate values of the oxygen partial pressure. That means, that the crystal morphogenesis and etching rate in an opened system are determined by the composition of silicate melt, as the medium, in which the migration of fluid (reagents and the products of diamond oxidation) takes place. The latter conclusion can be of great impor-

tance for the determination of natural diamonds' stability (conservation) during the formation of original diamond deposits.

Skublov S. G. & Drugova G. M. REE distribution in metamorphic garnets

Institute of Precambrian Geology and Geochronology, Saint-Petersburg, Russia skublov@ad.iggp.ras.spb.ru

key words: [*rare earth elements, garnets*]

A preliminary examination of trace and REE distribution patterns in the garnets from metamorphic rocks reveals an overall picture of their elements' behavior in the garnets during regional metamorphism [1, 2, 3]. In particular, all the garnets are found to be HREE-enriched, however, REE pattern of lower-Ca garnets markedly differs from that of higher-Ca garnets from the same complex, e.g. in the presence of a major negative Eu-anomaly. The paper deals with data on REE and trace elements abundances both for garnets derived from Lapland Granulite Belt (LGB) and aluminous schists from the supracrustal Korva-tundra suite which is adjacent to it on the south. REE and trace elements abundances were determined by INA technique.

Inhomogeneous granulite conditions were different in the southeastern (Salnye Tundry, 11,5–13 kbar and 1000°C), northeastern (River Lotta, 6 kbar and 900°C) and southwestern (River Javre, 9 kbar and 800°C) domains of LGB. Mafic schists derived from metamorphism of mafic igneous rocks are dominant among the Salnye Tundry granultites. In the Javre domain, the bulk rocks are garnet–sillimanite gneiss and quartzite-gneiss. In the Lotta domain, the granulite assemblage comprises cordierite-bearing garnet-sillimanite gneisses. The Upper Archaean supracrustal Korva-tundra suite comprises garnet-kyanite-biotite-muscovite schists. P-T parameters are defined to be 7–8 kbar and 550–650°C.

Two garnet groups from LGB mafic schists are distinguished based on REE-distribution pattern: the Salnye Tundry (samples C-7, C-29, C-49) and Javre (samples 621, 632) garnets (Fig. 1a). The latter show higher REE abundance and maximal Yb abundance (La/Yb = 0.06) as compared to the former. The Salnye Tundry garnets are depleted in REE and show minimal Sm abundance (La/Yb = 0.17-0.19). The sample C-49 differs from the above two garnets in an extremely high MgO-content and belongs to a subgroup of garnets derived from the igneous source rocks, probably, garnet peridotites. This garnet is depleted in REE as compared to two garnets mentioned, and shows maximal Ce- and minimal La- and Nd-abundances. It exhibits a rather high LREE/HREE ratio (La/Yb = 0.41). Judging from Figure 1a, the garnets from mafic schists in the Javre and Salnye Tundry domains (excluding sample C-49) show a similar curve of REE, the Javre garnets (with lower temperature formation) being, as a whole, REE-enriched. Different REE-distribution pattern is characteristic of the garnets derived from acid granulites, i.e. gneiss, quartzite-gneiss and granite (Fig. 1b). All the garnets show an intense Eu-anomaly, especially pronounced in quartzite-gneisses and granites. Eu/Eu* ratio falls into the 0.03–0.15 range. Besides, they are enriched in HREE,

their Tb and Yb concentrations being 120-100 times as high as the chondritic ones. La/Yb ratio in the garnets from quartzite-gneisses (samples 606, 627v) and granites (sample 629) is 0.07–0.13, and more differentiated (La/Yb = 0.34–0.66) in those from aluminous gneisses (samples 605, 619, 626, 250g). The garnets derived from the Korva-tundra kyanite-two-mica schists (samples 612, 633b; Fig. 1a) are found to exhibit quite different REE-distribution

pattern as compared to that of garnets from LGB acid granulites: despite a lower Ca-content of the garnets derived from the Korva-tundra schists, they lack Eu-anomaly pertinent to low-Ca garnets from other LGB domains. Their overall shape of REE distribution curve is most close to REE plotting garnets from the mafic Salnye Tundry, the only difference being expressed in higher La, Ce, Yb, and Lu (La/Yb = 0.08–0.29).
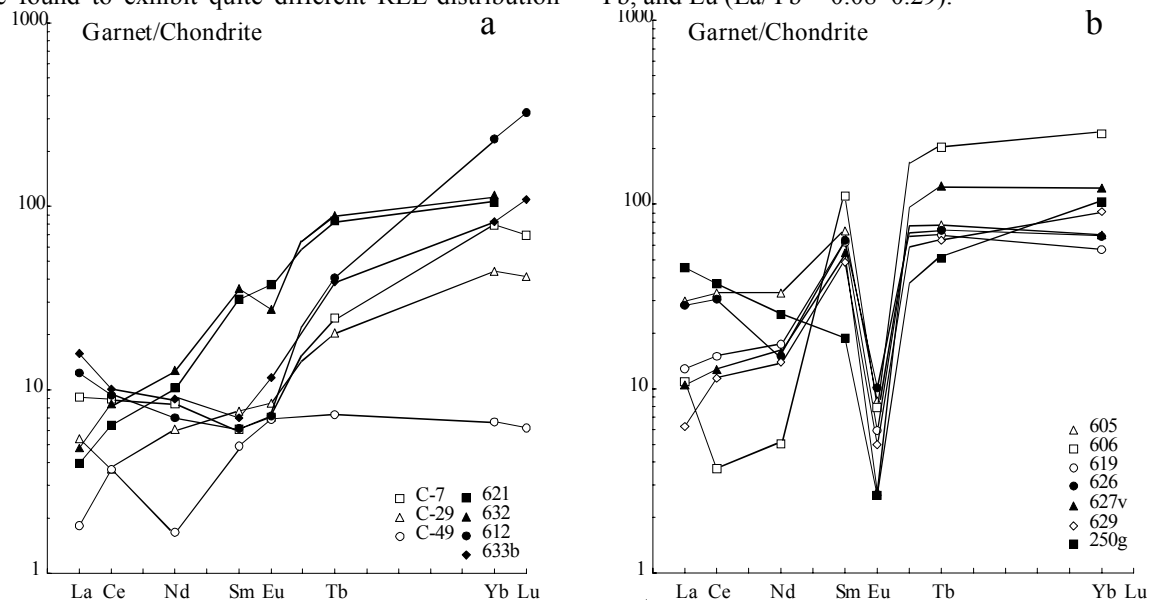
Fig. 1. Chondrite-normalised REE patterns for garnets from mafic schists (a) and acid granulites (b). Normalising coefficients from [4].

High-Ca Javre domain garnets reveal HREE enrichment as compared to those from their Salnye-Tundry analogs suggesting lower P-T parameters of the granulite metamorphism within the Javre domain. This conclusion is confirmed by the examination of the garnets from contact-metamorphic rocks in British Columbia [5]. The garnets showing prograde zoning derived from the increase in temperature accompanying with that of MgO-content and the decrease in MnO-content from the core towards crystal rim exhibit a regular depletion in HREE abundances.

REE-distribution patterns in the garnets from LGB allows to infer some conclusions.

1. The garnets from the mafic schists show a gentle slope of LREE/HREE enrichment and lacking Eu-anomaly. The garnets from the Javre schists are enriched in REE as compared to their Salnye Tundry analogs suggesting lower parameters of the granulite metamorphism within the latter.

2. Different shapes of REE-distribution curves in the garnets from the Salnye Tundry mafic schists are due to an extremely high-magnesian garnets of igneous origin whose non-differentiated REE distribution is similar to that of ultramafic rocks.

3. Lower-Ca garnets from the aluminous gneisses show HREE-enrichment and pronounced negative Eu-anomaly whose intensity tends to enhance with the increase in SiO_2-content of the host rock.

4. The increase in HREE abundances in the garnets is, at first, due to lowering temperature of their formation.
References:

1. Drugova, G.M., Shcheglova, T.P., Skublov, S.G., Savelieva, T.E., Krylov, I.N. 1998. To geochemistry of garnet in metamorphic rocks. *Proc. RMS.* 2: 72-85.
2. Hickmott, D.D., Shimizu, N., Spear, F.S., Selverstone, J. 1987. Trace element zoning in a metamorphic garnet. *Geology.* 15: 573-576.
3. Skublov, S.G., Drugova, G.M., Vrevsky, A.B. 2000. REE distribution in garnet from the Lapland Granulite Belt. *Proc. RMS.* In press.
4. Sun, S.S., Nesbitt, R.W. 1978. Petrogenesis of Archaean ultrabasic and basic volcanics: evidence from rare earth elements. *Contrib. Mineral. Petrol.* 65: 301-325.
5. Hickmott, D.D. & Shimizu, N. 1990. Trace element zoning in garnet from the Kwoiek Area, British Columbia: disequilibrium partitioning during garnet growth? *Contrib. Mineral. Petrol.* 104: 619-630.

Ostapenko G.T. Anisotropy assessment for growth rates of andalusite and sillimanite crystals (luring kyanite—>andalusite, kyanite—>sillimanite and andalusite—>sillimanite transformations.

Institute of Magnetism, National Academy of Sciences, 36-6, Vernadsky Ave., Kyiv, 252142, Ukraine ostap @ imag.kiev.ua

key words: [*andalusite, sillimanite, kyanite, transformation kinetics, crystal growth*]

In the paper published earlier [I], the following kinetic equations for kyanite (Ky)→andalusite (And), kyanite(Ky)→sillimanite(Sil) and andalusite(And) → sillimanite(Sil) transformations were derived by the author:

$$(dm/d\tau)_{Ky->And} = -5.96\bullet10^{-9}\exp(-E/RT) (P-P_*) \text{ mol/cm}^2\bullet\text{sec,}$$
(l)
$$(dm/d\tau)_{Ky->Sil}=-1.19\bullet10^{-9}\exp(-E/RT) (P-P_*) \text{ mol/cm}^2\bullet\text{sec,}$$
(2)
$$(dm/d\tau)_{And->Sil} =0.50\bullet10^{-9}\exp(-E/RT) (P-P_*) \text{ mol/cm2}\bullet\text{sec,}$$
(3)

where m is weight of a growing crystal (And or Sil); t - time; E - activation energy, which equals 112 ± 38 kJ/mol for the transformations mentioned above [1]; P and P_* - values of specific and equilibrium pressures of H_2O at the given temperature (for the Ky And, Ky Sil and And Sil equilibria respectively).

Linear dependence on $(P-P_*)$ and, respectively, on thermodynamic affinity of the reaction A ($A=-\Delta G_{reaction}=-\Delta V(P-P_*)$, where ΔV is volume change during the reaction) is observed within slight deviation from equilibrium [2]. Equation (1) - (3) were derived based on experimental study of the transformation degree (ξ) in mixtures, consisting of Ky + And, Ky + Sil and And + Sil grains (with addition of quartz particles). It was assumed that grains of the starting substances were of isometric (spherical) shape (of course, it was simplification due to prismatic appearance of the minerals, especially Ky and Sil) and grew in different directions with equal rates. Thorough microscopic studies of andalusite and sillimanite growth on their seed grains showed the highest build-up rates in the C direction (∥C axis,) and the lowest ones perpendicular to the C (⊥C axis). Faces, formed on the andalusite seed grains, resulted from a) relatively thick grown layer in the C direction (5-15 μm) most probably limited with {001} and {101} faces; b) very thin grown layer (1-3 μm) in ⊥_C direction likely bounded by {110} prism face. Roughly estimated, ratio of growth rates in ∥C and ⊥C directions, varies from 5 to 10. These results agree with data given [3], where it was shown that the same ratio for andalusite single crystal at the expense of kyanite grains dissolution equals ~**4-8,** that is, approximately 6, the value being very close to ones for small andalusite grains. Growing up of andalusite single crystal in the direction ∥C, that is growing of the {001} face, is classified as the adhesive growth mechanism on the kinked face and crystal accretion ⊥C (growing of the {110} face, which is to be classified as the flat one) is the layer-by-layer growth mechanism [3]. Sillimanite grains showed formation of sharp growth cones, contacting by the basements, in the C direction (instead of the continuous growth layer as in the case of andalusite) and extremely weak growth and formation of faces ⊥C (proved by formation of isolated growth cones). In the first approximation, ratio of growth rates in ∥C and ⊥C directions, is ≥10. It seems that the kyanite crystals can be characterized by similar values of crystallization anisotropy.

Statistics resulting from measurements of grain dimensions in the starting mixtures (being ~30 μm on average [1,2]) showed that width (m) and length (1), the latter usually being ∥C, average 25.5 μm and 44.5 μm for anda-lusite (1:m=1.59), 26,5 μm and 44.5 μm for sillimanite (1:m=1.68) and 20.8 μm and 53.5 μm for kyanite (1:m=2.57). Assuming these starting grains to be tetrahedral prisms (m*m*1), growth pyramids can be calculated on the faces ∥C and ⊥C. In this way, growth rates ∥C were calculated (instead of the averaged rate values in any direction (1) -(3)):

$$(dm/d\tau)_{Ky->And} = -10.86\bullet10^{-9}\exp(-E/RT) (P-P_*) \text{ mol/cm}^2\bullet\text{sec,}$$
(4)
$$(dm/d\tau)_{Ky->Sil}=-3.15\bullet10^{-9}\exp(-E/RT) (P-P_*) \text{ mol/cm}^2\bullet\text{sec,}$$
(5)
$$(dm/d\tau)_{And->Sil} =1.01\bullet10^{-9}\exp(-E/RT) (P-P_*) \text{ mol/cm2}\bullet\text{sec,}$$
(6)

It is useful to present the crystallization rate equations (4) - (6) as functions of thermodynamic affinity:

$$(dm/d\tau)_{Ky->And} = 14.59\bullet10^{-9}\exp(-E/RT)\bullet A (P-P_*) \text{ mol/cm}^2\bullet\text{sec,} \quad (7)$$
$$(dm/d\tau)_{Ky->Sil}=5.42\bullet10^{-9}\exp(-E/RT)\bullet A (P-P_*) \text{ mol/cm}^2\bullet\text{sec} \quad (8)$$
$$(dm/d\tau)_{And->Sil} =6.19\bullet10^{-9}\exp(-E/RT)\bullet A (P-P_*) \text{ mol/cm2}\bullet\text{sec,} \quad (9),$$
where A is in joules.

Growth rates ⊥C can be determined using (4) — (9) by dividing numerical coefficients by 6 (for Ky And transformation) and by 10 (for the Ky Sil and And Sil ones).

As follows from equations (7) - (9), at equal values of affinities 1) andalusite grows most quickly and sillimanite - most slowly, these rate ratios ranging 2.35 - 2.69; and 2) Ky Sil and And Sil transformation rates are essentially the same, pointing that the sillimanite crystallization rate (and not the kyanite and andalusite dissolution rates) is a controlling factor of the Ky Sil and And Sil transformations. It can be presumed, that kyanite crystallization rate is the limiting one in the Ky And transformation.

The obtained values of crystal growth rates for andalusite and sillimanite, as well as for the kyanite, can be used for time calculations during transformations between Al_2SiO_5-minerals (when they contact in metamorphic rocks [1]). The quantitative characteristics of dissolution and crystallization rates for the aluminosilicates dealt with in this paper and for other metamorphic minerals [4,5] are necessary for the development of a growth theory for porphyroblasts, being the volumetric bodies with different degree of idiomorphism.

References:

1. Ostapenko G.T. et al.(1992) / /Geochem. International, v. 29, N 2, pp. 1 - 10.
2. Ostapenko G.T. et al. (1997) // Geochem. International, v. 35, N 3, pp. 235 - 238.
3. Ostapenko G.T. et al. (1998) // J. Cryst. Growth, v. 186, pp. 420 - 426.
4. Murphy W.M., Helgeson H.C. . (1989) // Amer. J. Sci., V. 289, N 1, pp. 17-101.
5. Schramke J.A. et al. (1986) // Amer, J. Sci., v. 287, N 6, pp. 517 - 559.

Zhymulev E.I. Study of etching of diamonds in mantle rocks - xenolithes from kimberlites

Design and Technological Institute of Monocrystals, SB RAS,
Russkaya str., 43 Novosibirsk 630058 chepurov@crystal.nsib.ru

Dissolution of natural diamonds in the kimberlitic magma is one of the most disputable questions to date. Even more doubtful point in diamond genesis is the possibility of their dissolution in the mantle rocks, which are supposed to be their crystallization medium. Investigation of the inner morphology of diamond crystals frequently indicates at their complicated evolution, including the stages of dissolution.

This work is dedicated to the determination of the possibility of etching of diamonds in the presence of natural silicate minerals of mantle xenolithes from kimberlites. The experiments were held on a multy-anvil high-pressure apparatus of the "split-sphere" type, according to the technology, given in [1]. The flat-faced and sharp-edged natural octahedral and synthetic cubo-octahedral diamond crystals were used. For the silicate schist, the compositions from natural parageneses, corresponding to dunite, garnet lherzolite, spinel lherzolite, garnet pyroxenite, eclogite, served. The experiments with duration of 1 hr were carried out in hermetized platinum ampoules at 5.5-6.0 GPa, 1450-1500^{0}C.

Experimental conditions and results

Experiment No	Sample	Composition	Weight, mg (%)	Dia-monds (number)	Initial wieght, mg	End weight, mg	Etch figures
4-36-97	dunite	Ol Ga	108.6 (93) 8.2 (7)	1 natural	0.57	0.57	absent
7-28-98	eclogite	Cpx Ga	67.7 (60) 45.1 (40)	1 natural	0.57	0.53	present
7-9-99	spinel lher-zolite	Ol Opx Sp	95.0 (95) 3.0 (3) 2.0 (2)	1 natural	1.27	1.27	absent
7-14-99	garnet pyroxenite	Ga Cpx	73.45 (83) 15.0 (17)	2 synthetic	1.57	1.57	absent
8-25-99	garnet lherzolite	Ol Opx Ga	80.37 (82.7) 6.9 (7.1) 9.95 (10.2)	2 synthetic	1.43	1.39	present
8-30-99	eclogite	Ga Cpx	51.5 (50.7) 50.0 (49.3)	2 synthetic	1.54	1.49	present
8-37-99	spinel lherzolite	Ol Opx Sp	86.40 (81.3) 15.15 (14.3) 4.7 (4.4)	2 synthetic	1.48	1.48	present

In the experiments with dunite, garnet pyroxenite, the changes of crystals weight and morphology were not established. In case of other compositions, insignificant changes of the morphology and weight of crystals took place. In the experiments with spinel lherzolite, the changes related only to the micromorphology of crystal faces, while the weight loss was not determined. In case of garnet lherzolite, diamonds had lost 0,04 mg (2,8 %) of their weight. The most significant weight loss was fixed for diamond crystals in the experiments with eclogite: 7 and 3,2 %, the first value corresponding to the experiment with the higher content of pyroxene relative to garnet. The etch figures, which occurred in the experiments, are similar to those known for natural crystals and previously reproduced during diamond etching in silicate melts at the P-T parameters, corresponding to the field of thermodynamic stability of graphite [1]. At the {111} faces, the triangular etch pits, oriented reverse relative to the face outline (negative trigons), are most common. The flat-bottomed, as well as pyramid-shaped etch pits, 0,01-0,08 mm in size, were formed. Near the edges between octahedral faces, the etch layers in the form of parallel striation occurred. Near the edges between octahedral and cubic faces, the etch layers had "dentate" outline ("stairs-like pattern"). The incident angle between the "dents" was 60^0. The lateral parts of the layers, as well as those of the etch pits, were constituted by the surfaces, corresponding to trigon-trioctahedron. The {100} faces were etched with the exceptional formation of etch pits of rectangular outlines, parallel to the edges between octahedral and cubic faces. Besides, in the experiment No 8-37-99, the unusual etch figures appeared - flat, of various size, mainly rectangular, representing positive forms of the topography, lacking crystallographic orientation. Perhaps, they represent the prints of silicate phases during the etching.

As the melting of silicate melts was not reached in the experiments, the conclusion can be made, that it was the natural content of volatiles in silicate minerals, that accounted for diamond etching. The investigation, that was carried out, points to the principal possibility of diamonds' etching at the parameters of their thermodynamic stability, as well as to the composition of fluid, encapsulated in mantle minerals, being close to that, equiponderous to diamond.

Reference:

1. Chepurov A.I., Fedorov I.I., Sonin V.M. Experimental modeling of diamond formation processes. Novosibirsk: NIC UIGGM SB RAS Publishing House, 1997. 196 pp.